Defence Research and Development Canada
Recherche et développement pour la défense Canada

DEFENCE R&D DÉFENSE

Simulation of MC-CDMA systems

Minh-Quang Nguyen, Paul Fortier and Sébastien Roy

Defence R&D Canada – Ottawa
CONTRACT REPORT
DRDC Ottawa CR 2006-292
November 2006

Canada

Simulation of MC-CDMA systems

Minh-Quang Nguyen
Paul Fortier
Sébastien Roy

Prepared by:

Laboratoire de radiocommunications et de traitement du signal
Université Laval, Québec

Project Manager: Andrew Mudry
Contract Number: W7714-5-0942
Contract Scientific Authority: Jean-François Beaumont

Defence R&D Canada – Ottawa
Contract Report
DRDC Ottawa CR 2006-292
November 2006

Scientific Authority

Original signed by Jean-François Beaumont

Jean-François Beaumont

Approved by

Original signed by Darren Baker

Darren Baker
AH/Communications and Navigation Electronic Warfare

Approved for release by

Original signed by Cam Boulet

Cam Boulet
Chair/Document Review Panel

Abstract

Recently, Orthogonal Frequency Division Multiplexing (OFDM) has become a very attractive multicarrier transmission technique for wireless high speed data communications. OFDM offers robustness to multipath fading without having to provide powerful channel equalization. In order to support multiple users with high speed data communications, the Multi-Carrier Code Division Multiple Access (MC-CDMA) technique is used to address these challenges. MC-CDMA is a combination of OFDM and Code Division Multiple Access (CDMA) and has the benefits of both systems. Thus, the parameters of OFDM become the basic parameters of MC-CDMA. Simulations were performed for an MC-CDMA system under different channel environments. The simulation parameters considered were: guard time interval, symbol duration, sampling rate, and number of data subcarriers. The goal of the simulations was to allow for different MC-CDMA configurations to be tested in order to obtain the best system parameters. Simulations of MC-CDMA systems were also performed with different numbers of active users.

Résumé

Récemment, le multiplexage par division de fréquence orthogonale (MDFO) est devenu une technique très populaire de transmission multi porteuses pour les communications sans fil à haut débit. Le MDFO est robuste face aux évanouissements multi parcours sans avoir à recourir à de puissantes techniques d'égalisation. Afin de supporter de multiples usagers ayant de hauts taux de transmission, le système multi porteuses d'accès multiple par répartition de code (MP-AMRC) est utilisé pour répondre à ces défis. Le MP-AMRC est une combinaison du MDFO et de l'AMRC et a les avantages des deux systemes. Les paramètres du MDFO servent donc de paramètres de base au MP-AMRC. Des simulations ont été effectuées pour un systèmes MP-AMRC opérant sous différents types de canaux de communication. Les paramètres de simulation considérés furent : l'intervalle de garde, la durée du symbole, le taux d'échantillonnage et le nombre de sous-porteuses de données. Le but des simulations était de tester plusieurs configurations du MP-AMRC afin d'obtenir les meilleurs paramètres de système. Les simulations des systèmes MP-AMRC furent aussi effectuées pour un nombre différent d'usagers actifs.

This page intentionally left blank.

Executive summary

Simulation of MC-CDMA systems

Minh-Quang Nguyen, Paul Fortier, Sébastien Roy; DRDC Ottawa CR 2006-292; Defence R&D Canada – Ottawa; November 2006.

This work presents the simulation of a Multi-Carrier Code Division Multiple Access (MC-CDMA) system over multipath fading channels. Since the Code Division Multiple Access (CDMA) component of MC-CDMA is not defined yet, it was assumed for this work that Wideband CDMA (WCDMA) will be used. The use of different modulation schemes such as Quadrature Phase Shift Keying (QPSK), 16-Level Quadrature Amplitude Modulation (16QAM), and 64-Level Quadrature Amplitude Modulation (64QAM) along with the Orthogonal Frequency Division Multiplexing (OFDM) technique provide high speed data transmission over multipath fading channels. The channel models used are as specified in the Third Generation Partnership Project (3GPP) Technical Specification TS 25.101v2.10, namely indoor to outdoor/pedestrian and vehicular environments with a channel bandwidth of 5 MHz.

First, simulations of OFDM systems were performed in order to obtain basic parameters for MC-CDMA systems. Since variations of the multipath fading channel affect the performance of the system, knowledge of the channel is crucial. Pilot-symbol-aided-modulation (PSAM) is one of the well known techniques to estimate the channel state at pilot symbol positions. Comb-type pilot channel estimation is used under the assumption that the channel changes from one OFDM block to the next and estimates the channel at pilot frequencies. The frequency response of the channel at frequencies where pilot tones are not located can be interpolated using various interpolation techniques such as linear, spline, fast Fourier transform (FFT), or low pass filtering.

Second, based on the advantages of the OFDM technique and Wideband CDMA (WCDMA), MC-CDMA is a strong candidate for future Fourth Generation (4G) systems. MC-CDMA systems also employ coherent detection based on the use of comb-type channel estimation in order to obtain knowledge of the channel. Multi-user support in MC-CDMA is based on the principle of spreading in the frequency domain. Because WCDMA was used, Orthogonal Variable Spreading Factor (OVSF) codes were also assumed to be used in MC-CDMA. A spreading factor of 8 was also assumed. Thus, the MC-CDMA systems that were studied can service simultaneously up to 8 different users. Computer simulations of the MC-CDMA systems indicate that the bit error rate (BER) performance degrades as the number of active users increases. Given a channel bandwidth of 5 MHz, MC-CDMA systems can achieve a maximum average data rate of 900 kbps, 1.8 Mbps, and 2.7 Mbps per user for QPSK, 16QAM, and 64QAM, respectively.

Sommaire

Simulation of MC-CDMA systems

Minh-Quang Nguyen, Paul Fortier, Sébastien Roy; DRDC Ottawa CR 2006-292; R & D pour la défense Canada – Ottawa; novembre 2006.

Ce travail présente la simulation de systèmes multi porteuses d'accès multiple par répartition de code (MP-AMRC) dans des canaux avec évanouissements multi parcours. Parce que la composante AMRC du MP-AMRC n'est pas encore définie dans un standard, il fut supposé dans ce travail que l'AMRC à large bande sera utilisé. L'utilisation de différentes modulations comme la modulation de phase quaternaire, la modulation d'amplitude en quadrature (MAQ) à 16 niveaux (MAQ-16), la modulation MAQ-64 ainsi que de la technique de multiplexage par division de fréquence orthogonale (MDFO), permettent la transmission à hauts débits sur des canaux à évanouissements multi parcours. Les modèles de canaux utilisés sont décrits dans la spécification technique du programme de partenariat de troisième génération (3GPP) TS 25.101v2.10, soit les environnements intérieur/extérieur pédestre et véhiculaire avec une largeur de bande de canal de 5 MHz.

Premièrement, des simulations de systèmes de multiplexage par division de fréquence orthogonale (MDFO) ont été effectuées afin d'obtenir des paramètres de base pour les systèmes MP-AMRC. Puisque les variations de canal multi parcours affectent les performances du système, la connaissance du canal est cruciale. La modulation assistée par symboles pilotes (MASP) est une des techniques bien connues pour estimer l'état du canal aux positions des symboles pilotes. Cette estimation de canal par peigne de fréquence est utilisée en supposant que le canal change d'un bloc MDFO à un autre et évalue le canal aux fréquences pilotes. La réponse en fréquence du canal aux fréquences non-pilotes peut être interpolée en utilisant diverses techniques comme l'interpolation linéaire, les splines, la transformée de Fourier rapides (TFR) ou le filtrage passe-bas.

Deuxièmement, en se basant sur les avantages du MDFO et de l'AMRC, le MP-AMRC est un candidat solide pour les futurs systèmes de 4^{e} génération. Les systèmes MP-AMRC emploient également la détection cohérente basée sur l'utilisation de l'estimation par peigne de fréquence afin d'obtenir la connaissance du canal. Le support multiutilisateur en MP-AMRC est basé sur le principe d'étalement en fréquence. Puisque l'AMRC large bande fut utilisé, des codes orthogonaux à facteurs d'étalement variables furent aussi supposés être employés dans le MP-AMRC. Un facteur d'étalement de 8 fut également supposé. Donc, les systèmes MP-AMRC qui furent étudiés peuvent supporter 8 usagers simultanément. Les simulations par ordinateur des systèmes MP-AMRC indiquent que la performance de taux d'erreur binaire se dégrade à mesure que le nombre d'utilisateurs actifs augmente. Étant donné une largeur de bande de

canal de 5 MHz, les systèmes MP-AMRC pourraient atteindre un débit maximum de 900 kbps, 1.8 Mbps et 2.2 Mbps par usager lorsqu'on utilise des modulations en quadrature à 4, 16 et 64 niveaux, respectivement.

This page intentionally left blank.

Table of contents

List of figures

List of tables

1 Introduction

This report presents the simulation of a complete Multi-Carrier Code Division Multiple Access (MC-CDMA) system (modulation, transmission over multipath fading channel, reception, and demodulation). Since the Code Division Multiple Access (CDMA) component of MC-CDMA is not defined yet, it was assumed for this work that Wideband CDMA (WCDMA) will be used. The use of different modulation schemes such as Quadrature Phase Shift Keying (QPSK), 16-Level Quadrature Amplitude Modulation (16QAM), and 64-Level Quadrature Amplitude Modulation (64QAM) along with the Orthogonal Frequency Division Multiplexing (OFDM) technique provide high speed data transmission over multipath fading channels. The channel models used are as specified in the Third Generation Partnership Project (3GPP) Technical Specification TS 25.101v2.10, namely indoor to outdoor/pedestrian and vehicular environments [1].

Since variations of the multipath fading channel affect the performance of the system, knowledge of the channel is crucial for accurate signal demodulation. Pilot-symbol-aided-modulation (PSAM) is one of the well known techniques to estimate the channel state at pilot symbol positions. In an OFDM system, the channel estimation can be performed by either inserting pilot tones into all subcarriers of the OFDM symbol (time domain) with a given period, also know as block type-pilot channel estimation, or inserting pilot tones into each OFDM symbols (frequency domain), also known as comb-type pilot channel estimation [2, 3]. The block-type pilot channel estimation has been developed under the assumption of a slow fading channel (i.e. the channel transfer function does not change very rapidly). The comb-type pilot channel estimation has been developed under the assumption that the channel changes from one OFDM block to the next. The comb-type channel estimation estimates the channel at pilot frequencies. Then, the frequency response of the channel at frequencies where pilot tones are not located can be interpolated using various interpolation techniques such as linear, spline, Fast Fourier Transform (FFT), or low pass filtering [3].

Furthermore, if the multipath channel is time varying, the interpolation in the time domain must track variations of the channel. Based on the advantages of the OFDM technique and CDMA, MC-CDMA is a strong candidate for future Fourth Generation (4G) systems. MC-CDMA systems also employ coherent detection based on the use of pilot tones in order to obtain the knowledge of the channel (comb-type channel estimation). Multi-user support in MC-CDMA systems is based on the principle of spreading in the frequency domain. Because Wideband Code Division Multiple Access (WCDMA) is used, Orthogonal Variable Spreading Factor (OVSF) codes are assumed to be the MC-CDMA spreading codes. OVSF codes have good cross-correlation properties that preserve orthogonality between different users. MC-CDMA systems also use various modulation schemes in the indoor to outdoor and vehicular channel

environments [1]. Finally, this report shows computer simulation results of MC-CDMA systems with different numbers of active users.

2 Fundamentals of MC-CDMA

2.1 Overview of multi-carrier modulation and OFDM

In multi-carrier modulation, the data stream is divided into N subcarriers or subchannels of lower data rate. This can be seen as parallel transmission in the frequency domain. This scheme does not affect the total bandwidth W. Each subcarrier is spaced W/N apart, while the symbol duration T is increased by a factor of N [4]. This leads to the key idea in understanding OFDM which is the orthogonality of the subcarriers that allows simultaneous transmission on N subcarriers without interfering with each other. Figure 1 illustrates the basic blocks of an OFDM transmitter.

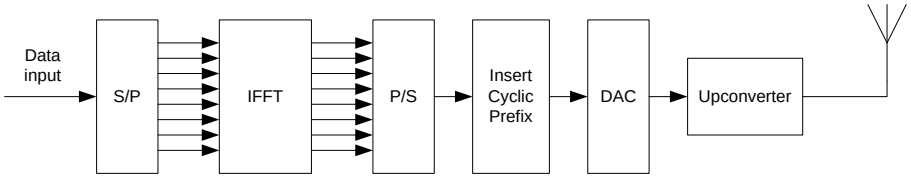

Figure 1: *Basic blocks of an OFDM transmitter.*

In OFDM, the input data is sent to a serial-to-parallel converter (the S/P block). Then, the N parallel outputs of the S/P block feed the inputs of the Inverse Fast Fourier Transform (IFFT) block in order to create an OFDM symbol, sometimes called the OFDM modulator. Since the subcarriers are orthogonal to each other, the OFDM symbol has overlapping sinc spectra centered at the subcarrier frequencies as shown in Figure 2 (Figure 4.5 in [4]). The individual subcarriers are separated and they do not mutually interfere.

After the IFFT has been computed, the N complex numbers at the output of the IFFT block are parallel-to-serial converted (P/S block). Then, the cyclic prefix is inserted in order to combat the inter-symbol interference (ISI) and inter-carrier interference (ICI) caused by the multipath channel. This cyclic prefix is sometimes called the guard interval. In order to create the cyclic prefix, the complex vector of length Δ at the end of the symbol duration T is copied and appended to the front of the signal block. The OFDM symbol duration then becomes $T_S = T + \Delta$ as shown in Figure 3 (Figure 4.8 in [4]). In practice, the cyclic prefix is chosen to be longer than the maximum delay spread of the channel.

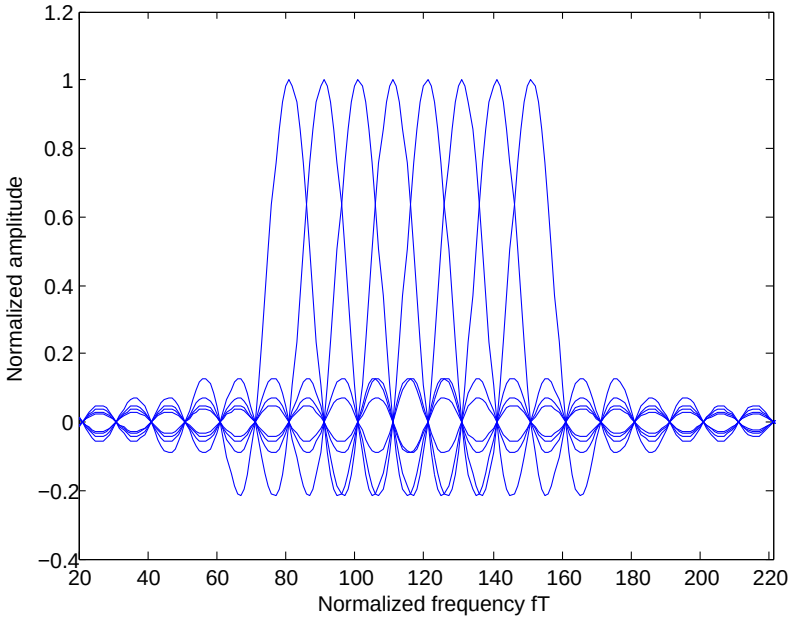

Figure 2: *Orthogonal overlapping spectral shapes for OFDM.*

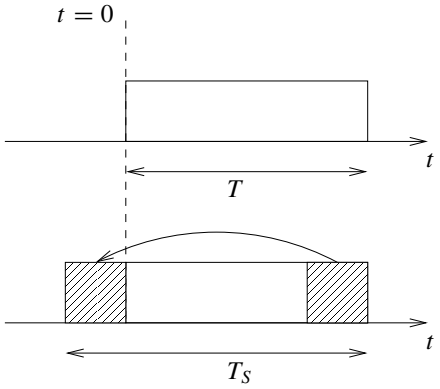

Figure 3: *Cyclic prefix of the OFDM symbol.*

Finally, the output of the cyclic prefix block is fed to the digital to analog converter (DAC) and lowpass filtered for each real and imaginary streams. The output of the DAC is upconverted, sent through a bandpass filter, and then sent to the antenna for transmission.

At the receiver side, the received signal is the convolution of the transmitted sequence and the channel impulse response. Figure 4 illustrates the basic blocks of an OFDM receiver. In the first step, the received signals are downconverted and fed to an analog to digital converter (ADC). Then, the removal of the cyclic prefix is performed by circular convolution [5] and the remaining samples are serial-to-parallel converted. The FFT block performs demodulation in order to obtain the transmitted symbols with the amplitude and phase corrupted by the channel response and the additive noise. The output bit stream is obtained by converting the output of the FFT block into a serial bit stream.

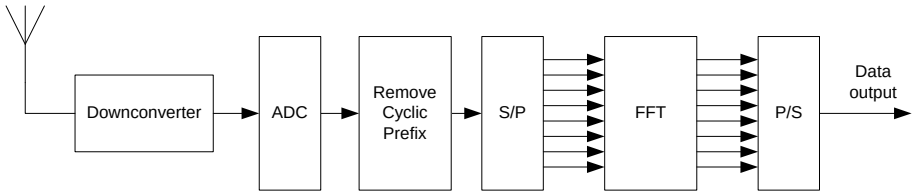

Figure 4: *Basic blocks of an OFDM receiver.*

2.2 Overview of CDMA

Code Division Multiple Access (CDMA) is a multiple access technique where different users share the same frequency band at the same time. Figure 5 illustrates an example of a simple CDMA transmission scheme.

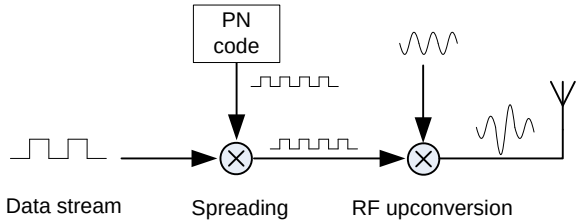

Figure 5: *Example of a simple CDMA transmitter.*

The heart of CDMA is the spread spectrum technique, which uses a higher data rate signature pulse to enhance the signal bandwidth far beyond what is necessary for a given data rate [4]. Spreading is obtained via a multiplication of the baseband data information by a spreading sequence of pseudorandom signs, sometimes called pseudonoise (PN) or code signal, before transmission. An example of spreading is illustrated in Figure 6.

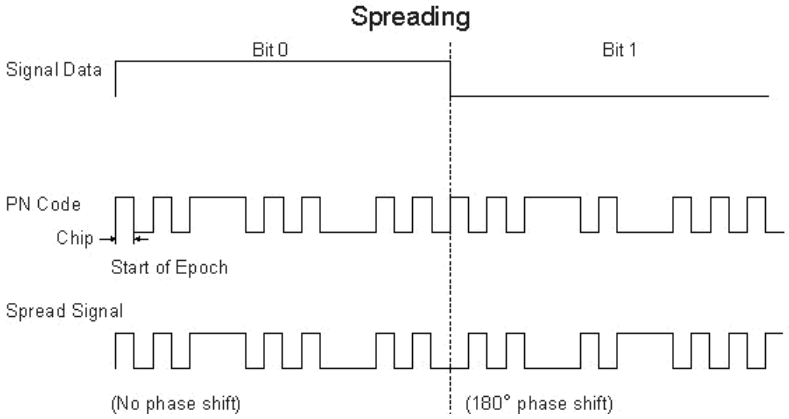

Figure 6: *Example of spreading in CDMA.*

The spreading factor (SF) is defined as the ratio of the information bit duration over the chip duration

$$G_{MC} = SF = \frac{T_b}{T_c} \tag{1}$$

where T_b and T_c are the bit duration and the chip duration, respectively. This leads to an increase of the bandwidth by the spreading factor, as shown in Figure 7.

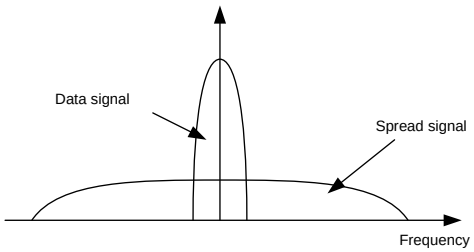

Figure 7: *Power spectrum of the spread signal versus the data signal.*

A spreading code is mainly characterized by its autocorrelation and cross-correlation functions. The rate of the spreading code is called the chip rate. A well known technique to generate the codes with a good autocorrelation property can be implemented using a linear feedback shift register (LFSR). A register of length m produces a sequence of "0"s and "1"s having maximal possible length $2^m - 1$, sometimes called maximal length sequence or m-sequence. In [4], the authors show that a linear feedback shift register of length m produces an m-sequence if and only if the corresponding generating polynomial of degree m is primitive. There are some useful codes with low cross-correlation based on m-sequences, such as Gold codes, Kasami codes, and Barker codes. For example, the Barker code of length $m = 11$ is used in the IEEE 802.11 wireless Local Area Network (LAN) standard.

2.3 Fundamentals of MC-CDMA

MC-CDMA, a novel digital modulation and multiple access scheme [6, 7], is a combination of OFDM and CDMA. Such a combination has the benefits of both OFDM and CDMA [4]. In MC-CDMA, symbols are modulated on many subcarriers to introduce frequency diversity instead of using only one carrier like in CDMA. Thus, MC-CDMA is robust against deep frequency selective fading compared to DS-CDMA [8]. Each user data is first spread using a given high rate spreading code in the frequency domain. A fraction of the symbol, corresponding to a chip of the spreading code, is transmitted through a different subcarrier [6].

2.3.1 MC-CDMA transmitter model

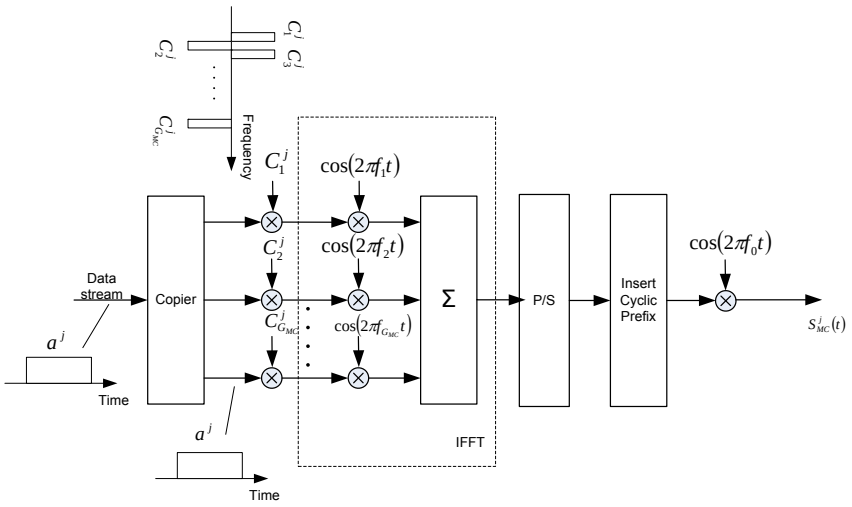

Figure 8: *MC-CDMA transmitter.*

The MC-CDMA transmitter configuration for the j^{th} user is shown in Figure 8. In this figure, the main difference is that the MC-CDMA scheme transmits the same symbol in parallel through several subcarriers whereas the OFDM scheme transmits different symbols. $c_j(t) = [c_1^j, c_2^j, ..., c_{G_{MC}}^j]$ is the spreading code of the j^{th} user in the frequency domain, G_{MC} denotes the processing gain, sometimes called the spreading factor. The input data stream is multiplied by the spreading code of length G_{MC}. Each chip of the code modulates one subcarrier. The number of subcarriers is $N = G_{MC}$. The users are separated by different codes. All data corresponding to the total number of subcarriers are modulated in baseband by an IFFT and converted back into serial data. Then, a cyclic prefix is inserted between the symbols to combat the inter-symbol interference (ISI) and the inter-carrier interference (ICI) caused by multipath fading. Finally, the signal is digital to analog converted and upconverted for transmission.

In MC-CDMA transmission, it is essential to have frequency non-selective fading over each subcarrier. Therefore, if the original symbol rate is high enough to become subject to frequency selective fading [6], the input data have to be serial-to-parallel converted into P parallel data sequences $[a_1^j, a_2^j, ..., a_P^j]$ and each serial-to-parallel output is multiplied with the spreading code of length G_{MC}. Then, each sequence is modulated using G_{MC} subcarriers. Thus, all $N = P \times G_{MC}$ subcarriers are also modulated in baseband by the IFFT. Figure 9 shows the modified version of the MC-CDMA transmitter.

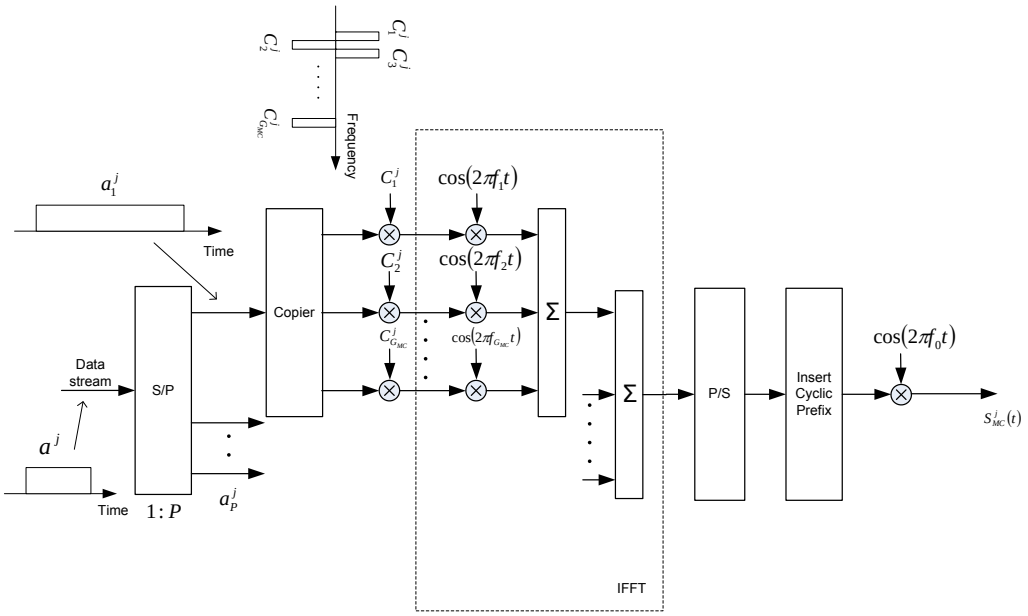

Figure 9: *Modified version of the MC-CDMA transmitter.*

In order to improve the performance of the system, an appropriate approach for channel estimation is to use dedicated pilot symbols that are periodically inserted in the transmission frame (in the time domain). This is known as block-type pilot channel estimation. The pilot tones can also be inserted into each symbol (in the frequency domain) with a given frequency spacing; this is known as comb-type pilot channel estimation [2, 3]. Block-type pilot channel estimation has been developed under the assumption of a slow fading channel(i.e. the channel transfer function does not change very rapidly). Comb-type pilot channel estimation has been developed under the assumption that the channel changes from one OFDM block to the other. Comb-type channel estimation estimates the channel at pilot frequencies. In comb-type pilot channel estimation, the frequency response of the channel, at frequencies where pilot tones are not located, can be interpolated using various interpolation techniques such as linear, spline, FFT, or low pass filtering [3]. Furthermore, pilot tones may be inserted in both time and frequency domains as shown in Figure 10 (Figure 4.35 in [4]) where the rectangular pilot insertion grid with pilot tones inserted every third frequency and every fourth time slot can be observed. The pilot density is thus $\frac{1}{12}$, that is, $\frac{1}{12}$ of the whole capacity is used for channel estimation.

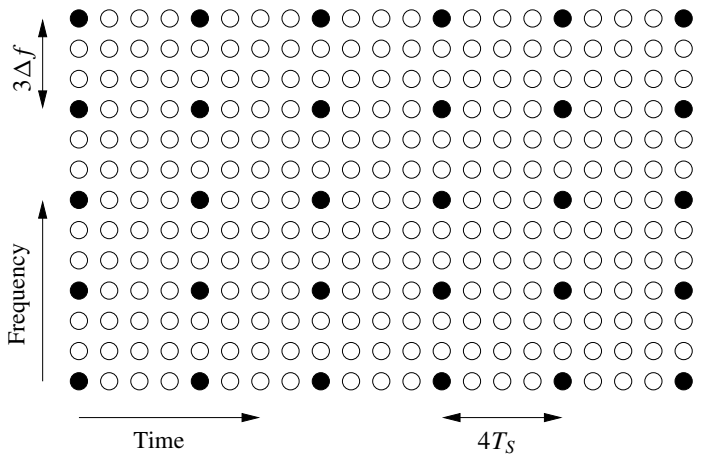

Figure 10: *Example of a pilot tone grid.*

2.3.2 MC-CDMA receiver model

The MC-CDMA receiver configuration for the j^{th} user is shown in Figure 11. The received signal is first downconverted. Then, the cyclic prefix is removed and the remaining samples are serial-to-parallel converted to obtain the m-subcarrier's components (corresponding to the a_P^j data), where $m = 1, 2, ..., G_{MC}$.

The m-subcarriers are first demodulated by a fast Fourier transform (FFT) (OFDM demodulation) and then multiplied by the gain q_m^j to combine the received signal

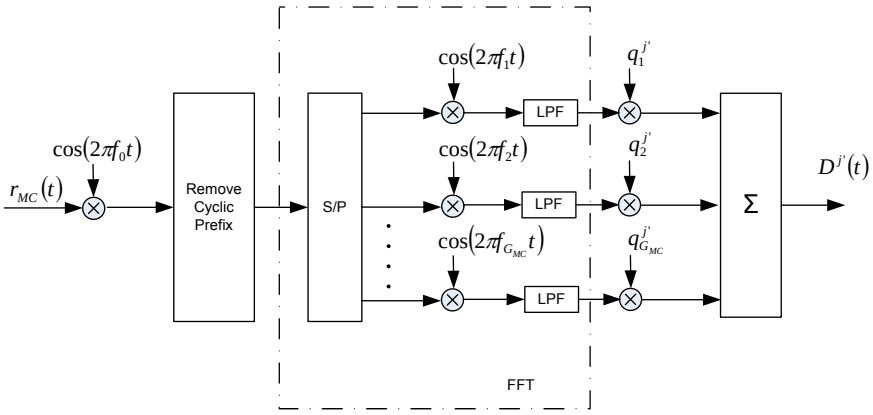

Figure 11: *MC-CDMA receiver.*

energy scattered in the frequency domain. In [6], the decision variable is given by

$$D^j = \sum_{G_{MC}}^{m=1} q_m y_m \tag{2}$$

with

$$y_m = \sum_{J}^{j=1} z_m^j a^j c_m^j + n_m \tag{3}$$

where y_m and n_m are the complex baseband components of the received signal and the complex Gaussian noise at the m^{th} subcarrier, respectively. z_m^j and a^j are the complex envelope of the m^{th} subcarrier and the transmitted symbol of the j^{th} user, respectively. J is the number of active users.

As mentioned in section 2.3.1, pilot symbols are periodically inserted in the transmission frame because coherent demodulation requires knowledge of the channel. The channel estimation is processed from the pilot symbols received at the beginning of each data frame. An optimum Wiener estimator is used [4, 9], and the channel estimation is processed across the time axis or the frequency axis or both. In order to obtain the channel estimation in two dimensions, a 2-D Wiener filter is derived and analyzed given an arbitrary sampling grid, an arbitrary selection of observations, and the possibility of a model mismatch [9]. Fortunately, the 2-D Wiener filter is simply implemented by using two cascaded orthogonal 1-D filters. This has been shown to

be virtually as good as a true 2-D filter. That is, the 1-D channel estimation is first performed, for example, along the frequency axis at the time slots where the pilots are located. At these time slots, there is a channel estimate available for every frequency. Then, the 1-D channel estimation along the time axis can be performed and an estimate for all time-frequency positions is available.

In the remaining sections of the report, simulations of MC-CDMA sytems prior to hardware implementations will be considered. The simulation of an OFDM system over several wireless channels plays a crucial role in the design of an MC-CDMA system. In the next section, two channel models will be considered: indoor to outdoor/pedestrian and vehicular [1]. Since there are no reference channel models provided yet for Fourth Generation (4G) wireless systems, channel models from the Third Generation Partnership Project (3GPP) will be used as reference.

3 3GPP TS 25.101v2.1.0 channel models

3GPP has modified the International Telecommunication Union (ITU) propagation models in order to use them for performance measurements in multipath fading channels. In Technical Specification TS 25.101v2.1.0, there are propagation condition models for indoor (Case 1), indoor to outdoor/pedestrian (Case 2), and for vehicular (Case 3) environments. All paths have a classical Doppler spectrum. Because the indoor to outdoor/pedestrian propagation model has a weaker average power for the second path than the indoor model at the same relative delay, the indoor to outdoor/pedestrian model was used as a worse case for a slow fading channel. The propagation conditions for indoor to outdoor/pedestrian and for vehicular environments with low delay spread are depicted in Figure 12 and Figure 13 (Case 2 and Case 3 in TS 25.101v2.1.0) [1]. A wireless channel bandwidth of 5 MHz was used in order to be consistent with the WCDMA bandwidth allocation. The carrier frequency is designated by the Universal Terrestrial Radio Access (UTRA) Absolute Radio Frequency Channel Number (UARFCN) [1].

3.1 Indoor to outdoor/pedestrian channel

In Figure 12, the first arrow represents the direct line of sight (LOS) signal, which is the strongest one and the reference level. The second arrow represents the first multipath signal, which is 12.5 dB weaker than the LOS signal and arrives 244 ns later. The third arrow represents the second multipath signal, which is 24.7 dB weaker than the LOS and arrives 488 ns later. Using this channel model, the following parameters were computed: maximum delay spread, mean excess delay, second moment of power delay profile, RMS delay spread, coherence bandwidth, and maximum Doppler spread.

The maximum delay spread of the channel is the maximum relative delay of the weakest multipath component as compared to the first arriving component in the power delay profile, sometimes called the maximum excess delay. This is an important parameter that is used to determine the guard interval for OFDM systems in a later section. Therefore, the maximum delay spread of this channel model is

$$\tau_{max} = 488 \text{ ns} \tag{4}$$

The mean excess delay is the first moment of the power delay profile and is defined as [10]

$$\bar{\tau} = \frac{\sum_k P(\tau_k)\tau_k}{\sum_k P(\tau_k)} = 0.0145 \ \mu\text{s} \tag{5}$$

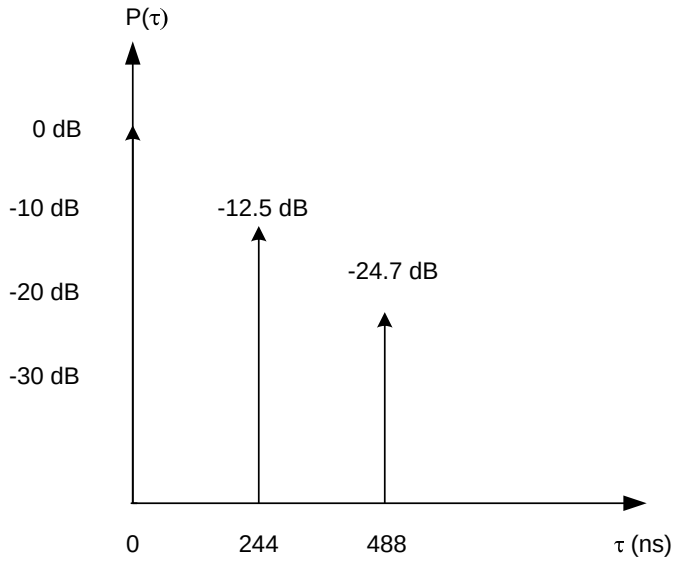

Figure 12: *Power delay profile for indoor to outdoor pedestrian environment (3 km/h).*

where $P(\tau_k)$ is the average power (in linear power units) and τ_k is the relative delay in seconds. The RMS delay spread is the square root of the second central moment of the power delay profile and is defined as [10]

$$\sigma_\tau = \sqrt{\bar{\tau^2} - (\bar{\tau})^2} \tag{6}$$

where $\bar{\tau^2}$ is the second moment of the power delay profile and is given by

$$\bar{\tau^2} = \frac{\sum_k P(\tau_k)\tau_k^2}{\sum_k P(\tau_k)} = 0.0039 \ \mu\text{s}^2 \tag{7}$$

Therefore, the RMS delay spread is

$$\sigma_\tau = \sqrt{0.0039 - 0.0145^2} = 0.0609 \ \mu\text{s} \tag{8}$$

The coherence bandwidth, B_C, is a statistical measure of the range of frequencies over which the channel can be considered "flat". If the coherence bandwidth is defined as the bandwidth over which the frequency correlation function is above 0.9 [10], then

$$B_C \approx \frac{1}{50 \times \sigma_\tau} \tag{9}$$

The coherence bandwidth is also an important parameter to determine subcarrier spacing for OFDM systems. In the indoor to outdoor case, the coherence bandwidth is approximately

$$B_C \approx \frac{1}{50 \times 0.0609 \times 10^{-6}} = 328.4 \text{ kHz} \tag{10}$$

The Doppler spread, f_D, is a measure of the spectral broadening caused by the time rate of change of the mobile radio channel and is defined as the range of frequencies over which the received Doppler spectrum is essentially non-zero. The maximum Doppler spread is given by [10]

$$f_D = \frac{v f_c}{c} \tag{11}$$

where v is the velocity of the mobile (3 km/h), f_c is the carrier frequency (f_c = 2160 MHz is set according to [1]), and c is the velocity of light.

$$f_D = \frac{3 \times 1000 \times 2160 \times 10^6}{3600 \times 3 \times 10^8} = 6 \text{ Hz} \tag{12}$$

The coherence time, T_C, is the time domain dual of the Doppler spread and is used to characterize the time varying nature of the frequency dispersiveness of the channel in the time domain and is defined as [10]

$$T_C = \frac{0.423}{f_D} = \frac{0.423}{6} = 0.0705 \text{ s} \tag{13}$$

The coherence time was used in the simulations to determine how many symbols can be transmitted while the channel remains constant.

3.2 Vehicular channel

For the vehicular case, the same parameters were essentially recalculated as for the previous case, but based on the power delay profile for the vehicular environment. These parameters were used to determine the system performance under this environment. Figure 13 shows a representation of the power delay profile. Notice that this profile contains more multipath signals than the previous case (Figure 12). Therefore, the vehicular case is a much more severe environment and system performance is expected to be degraded. Using this channel model, the following parameters were obtained.

Maximum delay spread:

$$\tau_{max} = 1708 \text{ ns} \tag{14}$$

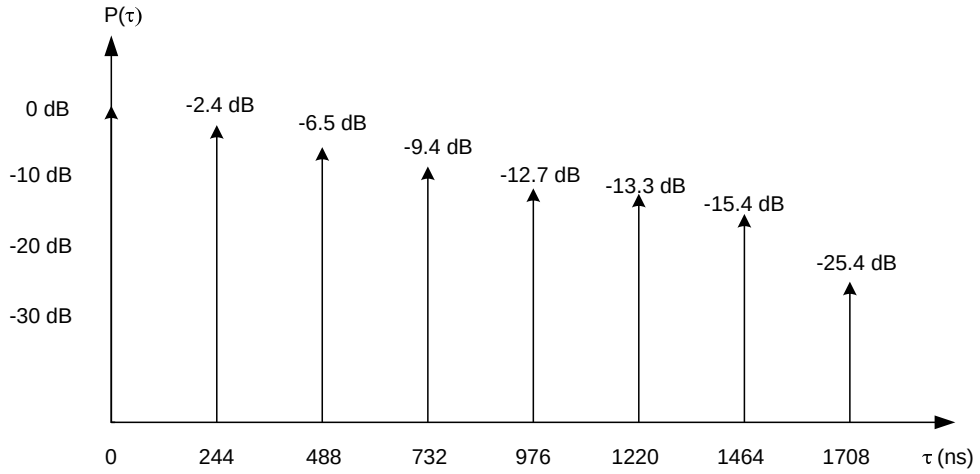

Figure 13: *Power delay profile for vehicular environment (120 km/h).*

Mean excess delay:

$$\bar{\tau} = \frac{\sum_k P(\tau_k)\tau_k}{\sum_k P(\tau_k)} = 0.2396 \ \mu\text{s} \tag{15}$$

RMS delay spread:

$$\sigma_\tau = \sqrt{\bar{\tau^2} - (\bar{\tau})^2} = 0.3298 \ \mu\text{s} \tag{16}$$

where the second moment of the power delay profile is

$$\bar{\tau^2} = \frac{\sum_k P(\tau_k)\tau_k^2}{\sum_k P(\tau_k)} = 0.1662 \ \mu\text{s}^2 \tag{17}$$

Coherence bandwidth:

$$B_C \approx \frac{1}{50 \times \sigma_\tau} = \frac{1}{50 \times 0.0609 \times 10^{-6}} = 60.64 \text{ kHz} \tag{18}$$

Maximum Doppler spread, assuming a vehicular speed of 120 km/h

$$f_D = \frac{120 \times 1000 \times 2160 \times 10^6}{3600 \times 3 \times 10^8} = 240 \text{ Hz} \tag{19}$$

Coherence time:

$$T_C = \frac{0.423}{f_D} = \frac{0.423}{240} = 0.0018 \text{ s} \tag{20}$$

Table 1 summarizes some important parameters of 3GPP channels.

Table 1: *Parameters for indoor to outdoor/pedestrian and vehicular channels.*

Parameters	Indoor to outdoor/pedestrian	Vehicular
Maximum delay spread (μs)	0.488	1.708
Mean excess delay (μs)	0.0145	0.2396
RMS delay spread (μs)	0.0609	0.3298
Coherence bandwidth (kHz)	328.4	60.64
Coherence time (s)	0.0705	0.0018
Maximum Doppler spread (Hz)	6	240

The simulations of 3GPP channels used Young and Beaulieu's method [11] for generating Rayleigh random variables. Figures 14 and 15 show the output fading envelopes of the first path of the indoor to outdoor/pedestrian and vehicular channels, respectively.

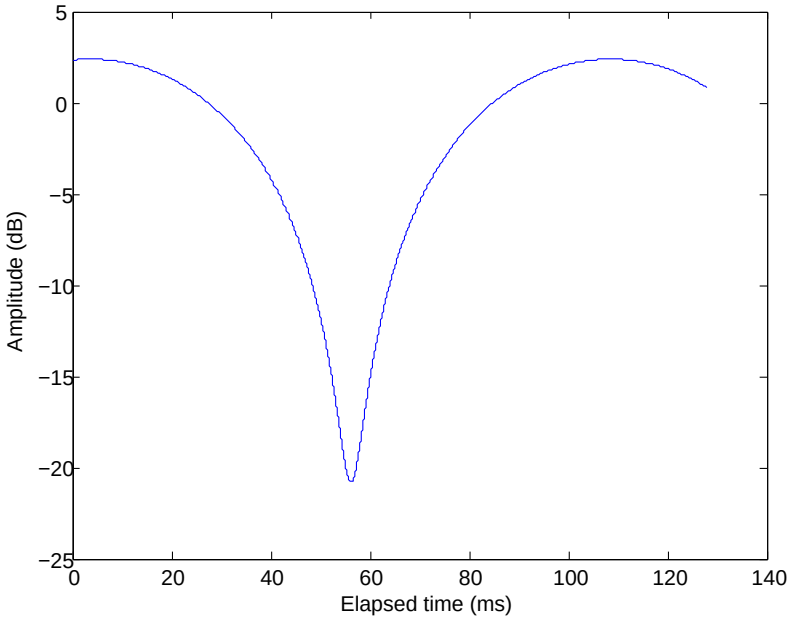

Figure 14: *Fading envelope for the indoor to outdoor channel.*

Figure 14 is a representation of the received signal variation over time as the mobile user moves at a speed of 3 km/h in an indoor/outdoor pedestrian environment. The signal is expected to vary over a relatively long interval (i.e. slowly). Figure 15 is a representation of the received signal variation over time for a mobile user at a speed of 120 km/h in a vehicular environment. The figure clearly shows that the received signal is expected to experience stronger and faster variations in shorter time intervals.

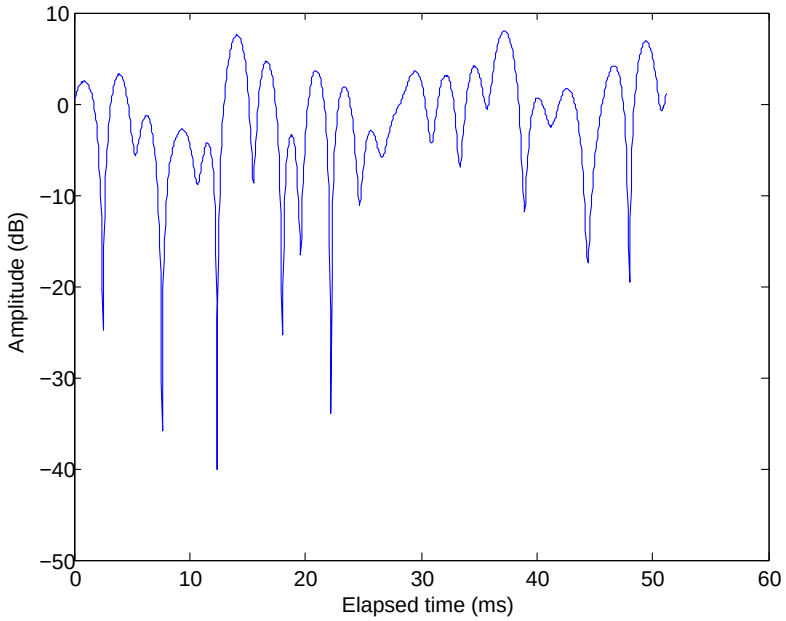

Figure 15: *Fading envelope for the vehicular channel.*

Again, this is an indication that lower performance is expected for the vehicular case since it is a much more severe environment.

4 OFDM simulation parameters

4.1 Indoor to outdoor/pedestrian channel

It is well known that one of the advantages of OFDM is the conversion of a frequency selective fading channel into a number of flat fading subchannels (narrow band signals). Thus, the bandwidth of an individual subchannel (subcarrier) Δf should be much less than the coherence bandwidth $B_C = 328.4$ kHz to ensure that the channel frequency response within the signal bandwidth is approximately constant [10, 12]. Given a channel bandwidth $BW = 5$ MHz, the FFT sampling rate was set to $F_s = 5$ MHz. Considering an FFT length of 64, the subcarrier spacing is

$$\Delta f = \frac{F_s}{N_{FFT}} = \frac{5 \times 10^3}{64} = 78.125 \text{ kHz} \tag{21}$$

The subcarrrier spacing is about one quarter of the coherence bandwidth $B_C = 328.4$ kHz, which is sufficient to consider the channel frequency response within the signal bandwidth to be approximately constant. Increasing the FFT length above 64 leads to hardware resource overhead and added system complexity. Therefore, the choice of an FFT length of 64 is appropriate in this case. Thus, the effective symbol duration (FFT interval duration) is

$$T = \frac{1}{\Delta f} = 12.8 \ \mu\text{s} \tag{22}$$

In [13], the author states that the guard time interval GI should be at least 4 times the maximum delay spread τ_{max} as a rule of thumb. Using this rule, the guard time in this channel environment is $GI = 4 \times 488$ ns ≈ 2 μs. However, in practical systems, the guard time interval is often taken to be 25% of the effective symbol duration. This duration of the guard interval implies an SNR loss of about 1 dB. For example, the guard interval in the IEEE 802.11a wireless LAN standard is $GI = 0.8$ μs which is 25% of the effective symbol duration, $T = 3.2$ μs [14]. Therefore, the guard interval was set to 25% of the effective symbol duration in this report. That is

$$GI = \frac{T}{4} = 3.2 \ \mu\text{s} \tag{23}$$

The guard interval is more than 4 times the maximum delay spread ($\tau_{max} = 0.488$ μs). Thus, the OFDM symbol duration can be expressed as

$$T_S = T + GI = 12.8 \ \mu\text{s} + 3.2 \ \mu\text{s} = 16 \ \mu\text{s} \tag{24}$$

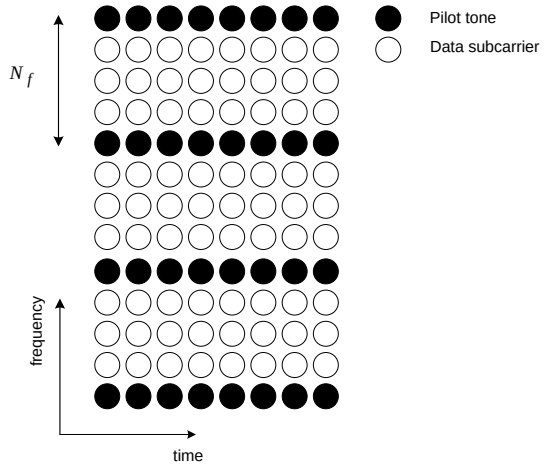

Figure 16: *Comb type pilot tones arrangement.*

Pilot-symbol-aided-modulation (PSAM) is one of the well known techniques for estimating the channel state at pilot symbol positions. As mentioned in section 2.3, the pilot tones are periodically inserted into several dedicated subcarriers of each OFDM symbol (comb-type pilot) as shown in Figure 16. The spacing between pilot tones in the frequency domain is denoted by N_f. Given the normalized channel bandwidth $\tau_{max}\Delta f$, the sampling theorem states that [9]

$$\tau_{max}\Delta f.N_f \leq 1/2 \tag{25}$$

Thus,

$$N_f \leq \frac{0.5}{\tau_{max}\Delta f} \approx 13 \tag{26}$$

The symbol rate is equal to the total number of subcarriers divided by the OFDM symbol duration. Because of the insertion of pilot tones into the OFDM symbol, the actual symbol rate can be expressed as

$$R_s = \frac{N_C}{T_S} \tag{27}$$

where N_C is the number of data subcarriers. Then, the maximum bit rate is

$$R_b = R_s \times \log_2 M \tag{28}$$

where $M = \{4, 16, 64\}$ is the constellation size of the modulation.

The occupied bandwidth is defined as the total bandwidth used by the system. That is

$$BW_{occ} = (\text{Number of subcarriers used} + 1 \text{ DC}) \times \Delta\text{f} \tag{29}$$

The bandwidth efficiency can be express as

$$BW_{eff} = \frac{R_b}{BW_{occ}} \text{ bits/s/Hz} \tag{30}$$

Table 2 shows the simulation parameters for the OFDM system over the indoor to outdoor channel environment with pilot tone spacings of $N_f = 8$ and $N_f = 12$ as show in figures 17 and 18, respectively. Table 3 shows the bandwidth efficiency of the OFDM system for this channel.

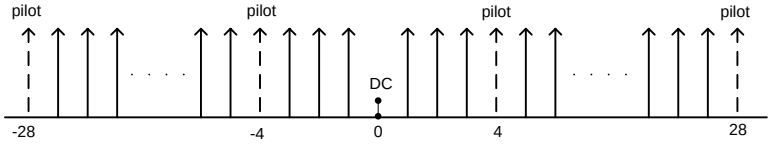

Figure 17: *Frequency allocation of subcarriers($N_f = 8$).*

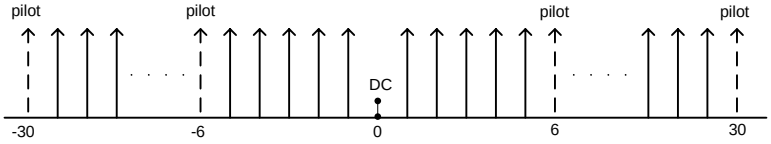

Figure 18: *Frequency allocation of subcarriers($N_f = 12$).*

Table 2: *Simulation parameters for the indoor to outdoor/pedestrian environment.*

Available bandwidth	5 MHz	
FFT sampling rate	5 MHz	
FFT size	64	
Effective symbol duration	12.8 μs	
Guard time duration	3.2 μs	
OFDM symbol duration	16 μs	
Subcarrier spacing	78.125 kHz	
Pilot spacing	8	12
Number of pilot tones	8	6
Number of data subcarriers	48	54
Number of subcarriers	56	60
Occupied bandwidth	4.45 MHz	4.76 MHz
Actual symbol rate	3 MSps	3.375 MSps

Table 3: *Bandwidth efficiency of OFDM system for the indoor to outdoor/pedestrian environment.*

Pilot spacing	8	12
QPSK	6 Mbps 1.35 bits/s/Hz	6.75 Mbps 1.41 bits/s/Hz
16QAM	12 Mbps 2.7 bits/s/Hz	13.5 Mbps 2.82 bits/s/Hz
64QAM	18 Mbps 4.04 bits/s/Hz	20.25 Mbps 4.25 bits/s/Hz

4.2 Vehicular channel

The simulation parameters for the OFDM system in the vehicular channel were calculated in the same way as for the indoor to outdoor channel. Given a channel bandwidth $BW = 5$ MHz, the FFT sampling rate was set to $F_s = 5$ MHz. Considering an FFT length of 256, the following values were obtained for the parameters.

Subcarrier spacing:

$$\Delta f = \frac{F_s}{N_{FFT}} = \frac{5 \times 10^3}{256} = 19.5313 \text{ kHz} \tag{31}$$

Effective symbol duration:

$$T = \frac{1}{\Delta f} = 51.2 \ \mu\text{s} \tag{32}$$

Guard interval:

$$GI = \frac{T}{4} = 12.8 \ \mu\text{s} \tag{33}$$

OFDM symbol duration:

$$T_S = T + GI = 51.2 \ \mu\text{s} + 12.8 \ \mu\text{s} = 64 \ \mu\text{s} \tag{34}$$

Pilot tone spacing:

$$N_f \leq \frac{0.5}{\tau_{max} \Delta f} \approx 15 \tag{35}$$

Table 4 shows the simulation parameters for the OFDM system over the vehicular environment with pilot tone spacings of $N_f = 8$ and $N_f = 12$ as shown in figures 19 and 20, respectively. The two figures are almost the same as figures 17 and 18, except for the FFT lengths. Pilot tone spacings of $N_f = 8$ and $N_f = 12$ were used in order to compare the performance of this system with the previous case (indoor to outdoor). Table 5 shows the bandwidth efficiency of the OFDM system for this channel.

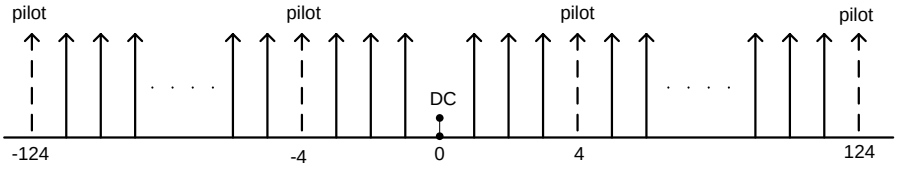

Figure 19: *Frequency allocation of subcarriers ($N_f = 8$).*

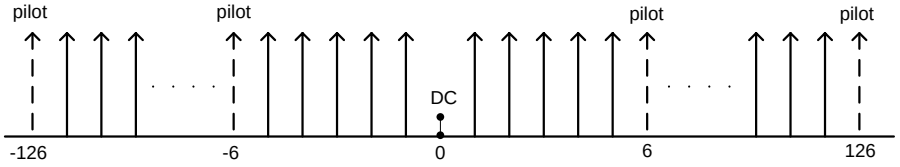

Figure 20: *Frequency allocation of subcarriers ($N_f = 12$).*

Table 4: *Simulation parameters for the vehicular environment.*

Available bandwidth	5 MHz	
FFT sampling rate	5 MHz	
FFT size	256	
Effective symbol duration	51.2 μs	
Guard time duration	12.8 μs	
OFDM symbol duration	64 μs	
Subcarrier spacing	19.5313 kHz	
Pilot spacing	8	12
Number of pilot tones	32	22
Number of data subcarriers	216	230
Number of subcarriers	248	252
Occupied bandwidth	4.86 MHz	4.94 MHz
Actual symbol rate	3.375 MSps	3.59 MSps

Table 5: *Bandwidth efficiency of OFDM system for the vehicular environment.*

Pilot spacing	8	12
QPSK	6.75 Mbps 1.39 bits/s/Hz	7.18 Mbps 1.45 bits/s/Hz
16QAM	13.5 Mbps 2.78 bits/s/Hz	14.36 Mbps 2.9 bits/s/Hz
64QAM	20.25 Mbps 4.17 bits/s/Hz	21.54 Mbps 4.35 bits/s/Hz

5 OFDM simulation

5.1 OFDM simulation model

Figure 21 shows the simulation block diagram for the QPSK-OFDM system. 16QAM and 64QAM modulations were also used. In the simulations, comb-type channel estimation was used in order to estimate the channel at pilot frequencies. Interpolation of the frequency response of the channel at the other frequencies using spline and lowpass Finite Impulse Response (FIR) interpolation techniques were also used. The Matlab software was selected as the simulation tool to implement the OFDM simulation model and all other models in this report. The following toolboxes were required in Matlab 7.1 to implement the OFDM simulation model.

- Signal Processing Toolbox
- Communications Toolbox

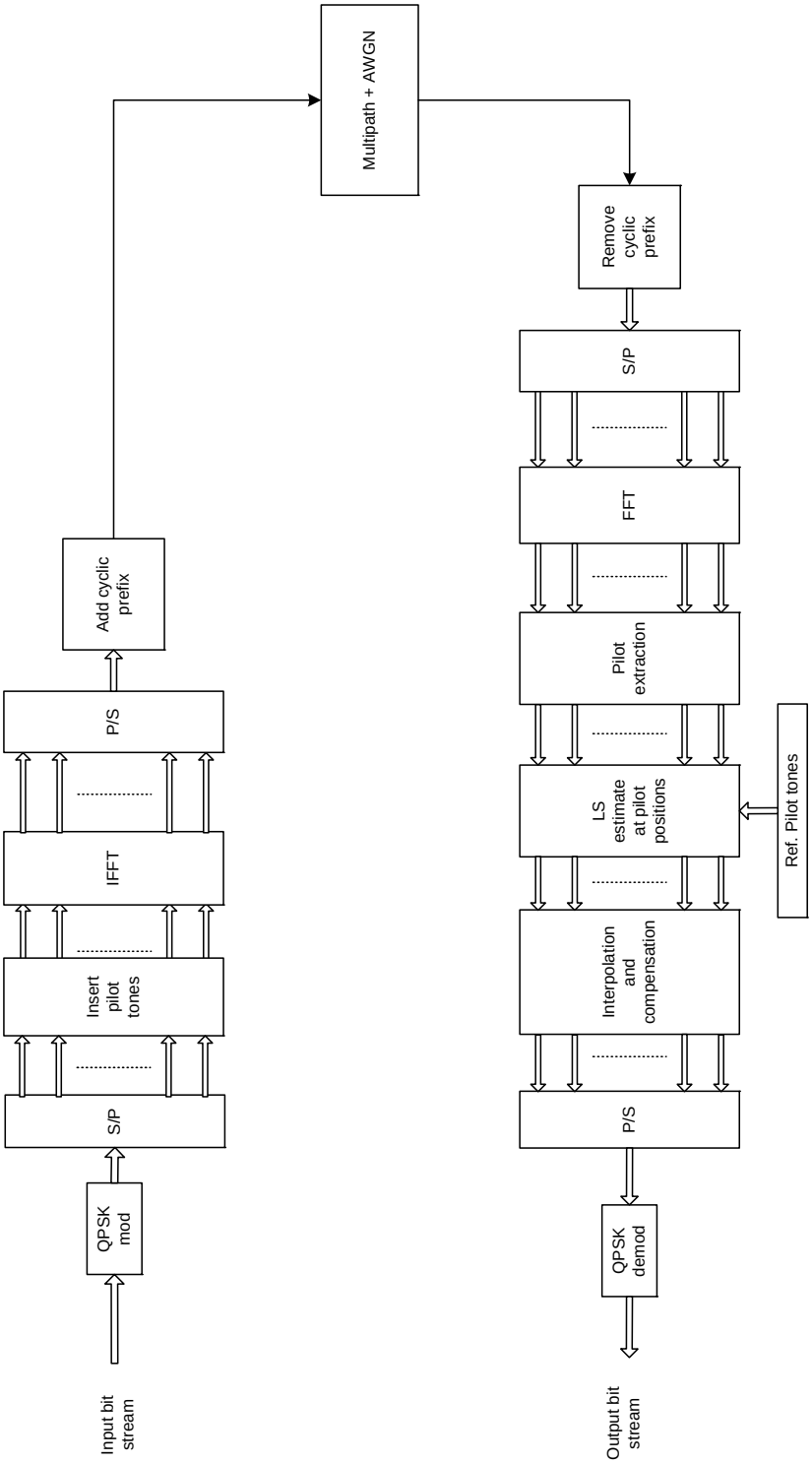

Figure 21: *Simulation block diagram for QPSK-OFDM.*

5.2 OFDM simulation results

Simulations were run to determine and analyze the performance of the systems under various configurations. The bit error probability as a function of the signal-to-noise ratio was calculated and illustrated graphically for the QPSK-, 16QAM-, and 64QAM-OFDM systems over the indoor to outdoor/pedestrian and vehicular channels. The channel estimation uses the spline and lowpass FIR interpolation methods with different pilot tone spacing.

5.2.1 Results for indoor to outdoor/pedestrian channel

Figures 22, 23 and 24 show the bit error probability as a function of the signal-to-noise ratio for the QPSK-, 16QAM- and 64QAM-OFDM systems over the indoor to outdoor channel. In these figures, the same representation of the curves was used for two sets of figures, one for spline interpolation and another for lowpass FIR interpolation. The solid curves represent the performances for the Additive White Gaussian Noise (AWGN) channel. A simple AWGN channel was used as a benchmark for all BER vs. E_b/N_0 curves. The solid curves with diamond markers represent performance of the system using perfect knowledge of the channel. The solid curves with upward-pointing triangle markers represent performance of the system with $N_f = 8$. Similarly, the solid curves with circle markers represent performance of the system with $N_f = 12$.

First, the performance of the QPSK-OFDM system in Figure 22 are considered. In this figure, the performance with perfect knowledge of the channel is very close to the AWGN curve. The curves with $N_f = 8$ and $N_f = 12$ are also very close. Figure 22 also shows that the difference between the perfect estimation curve and the interpolation curves is constant at about 2.4 dB for spline interpolation and 2.1 dB for lowpass FIR interpolation. A small performance difference between lowpass FIR interpolation and spline interpolation can also be observed. For example, consider a BER of 10^{-3} with $N_f = 8$; the difference is about 0.3 dB. The curves for 16QAM-, and 64QAM-OFDM also show similar performance differences between the perfect estimation and the interpolation curves.

However, the performance of 16QAM-, and 64QAM-OFDM are degraded as expected, meaning that for a given value of BER, a higher order modulation scheme requires a larger signal-to-noise ratio. For example, consider a BER of 10^{-3} with lowpass FIR interpolation and $N_f = 8$. From figures 22, 23, and 24, one can observe that the QPSK-, 16QAM-, and 64QAM-OFDM systems require a value of E_b/N_0 of about 8.7 dB, 13.3 dB, and 17.5 dB, respectively. Furthermore, since the lowpass FIR interpolation is easier to implement in digital circuits than the spline interpolation, the simualtion results for the lowpass FIR interpolation will be considered as references for future Field Programmable Gate Array (FPGA) implementations.

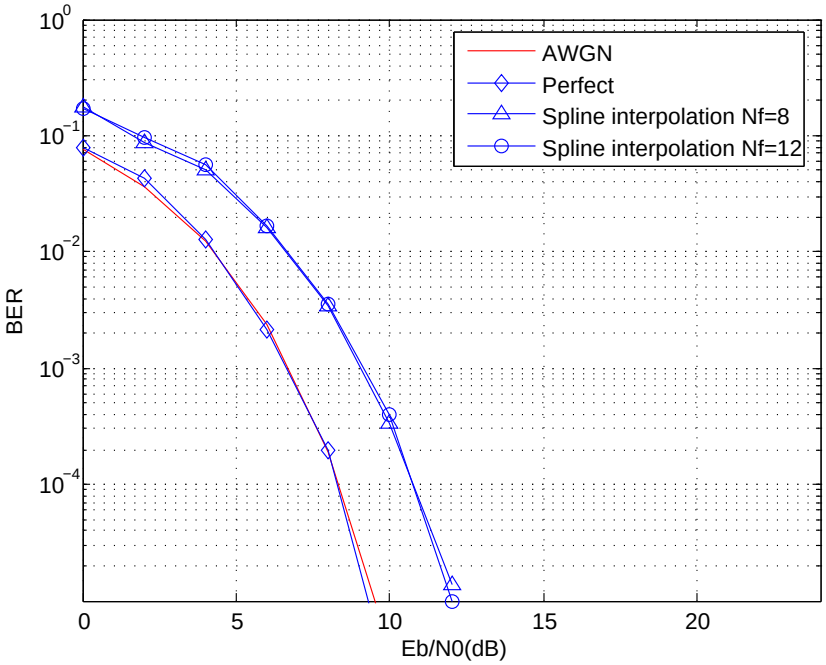

(a) Spline interpolation.

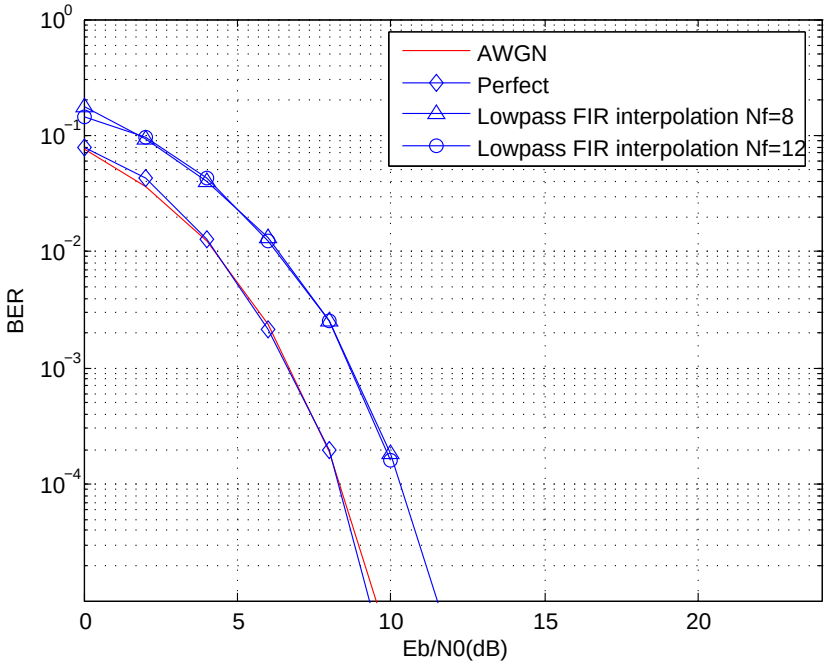

(b) Lowpass FIR interpolation.

Figure 22: *Performance of the QPSK-OFDM system over the indoor to outdoor channel.*

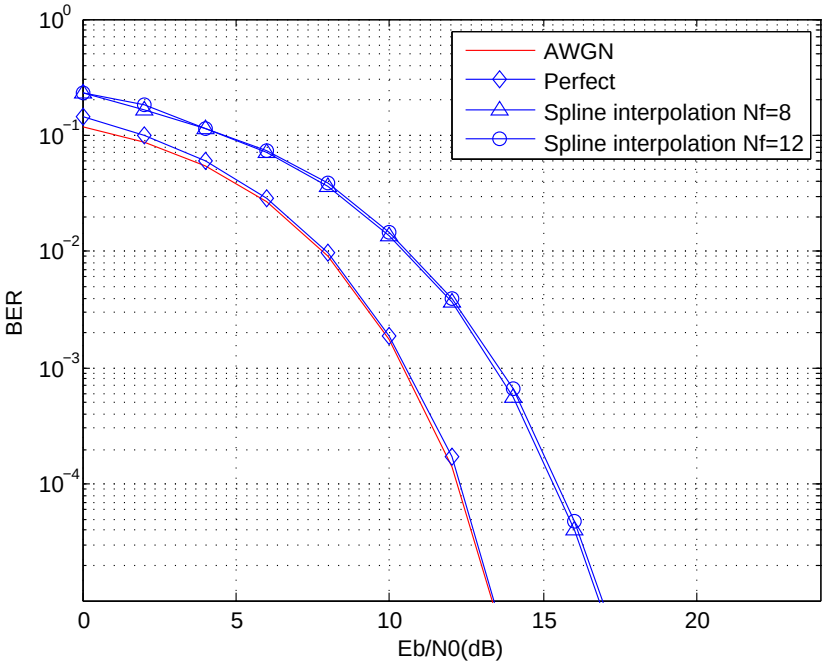

(a) Spline interpolation.

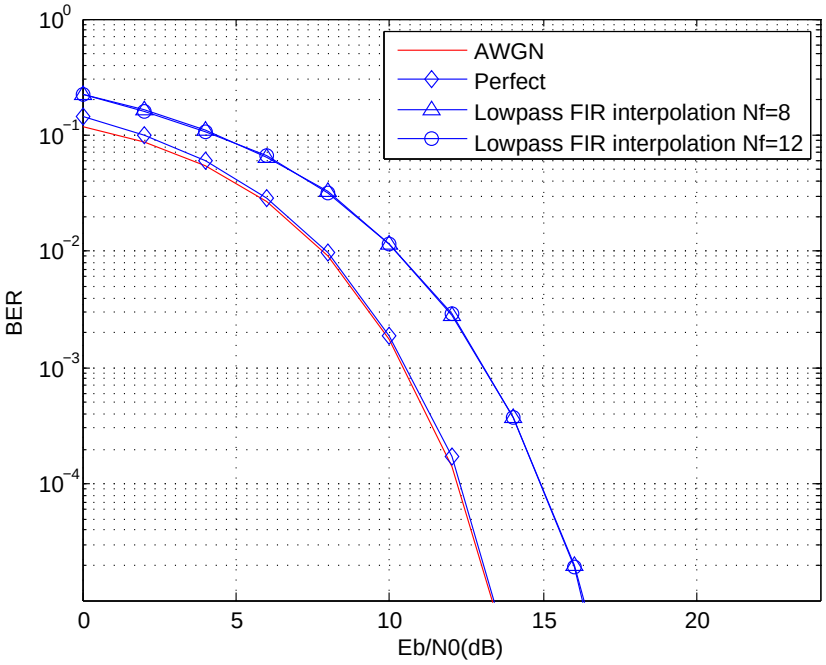

(b) Lowpass FIR interpolation.

Figure 23: *Performance of the 16QAM-OFDM system over the indoor to outdoor channel.*

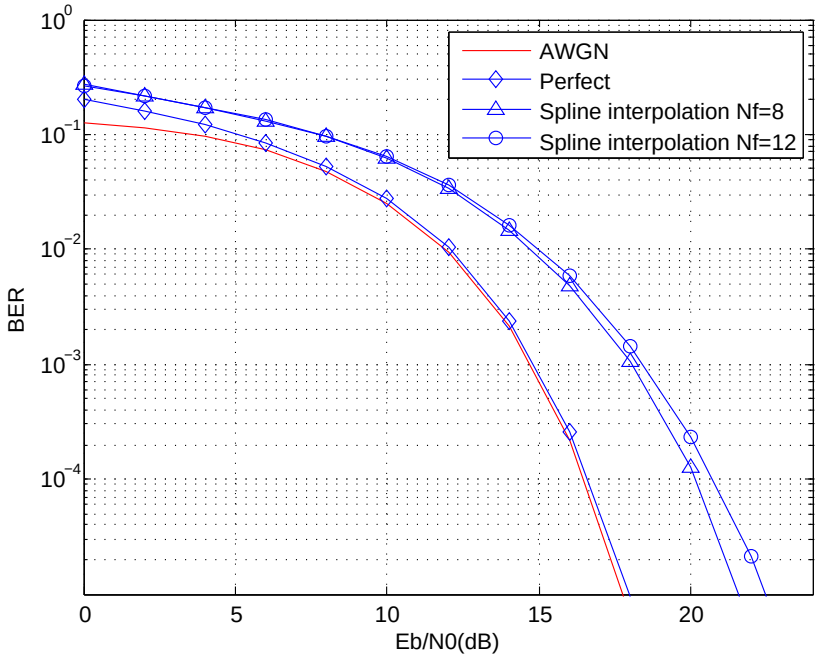

(a) Spline interpolation.

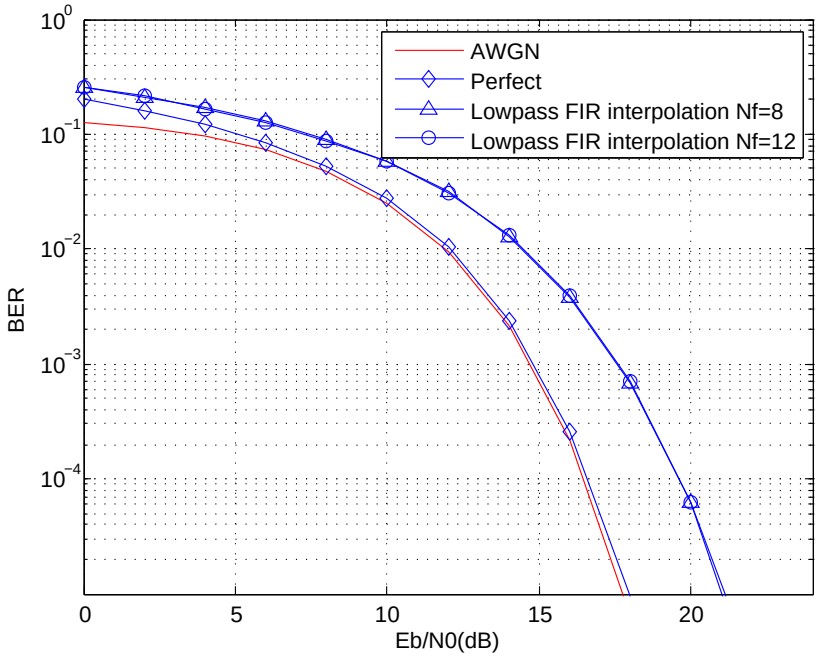

(b) Lowpass FIR interpolation.

Figure 24: *Performance of the 64QAM-OFDM system over the indoor to outdoor channel.*

5.2.2 Results for vehicular channel

Figures 25, 26 and 27 show the performances of QPSK-, 16QAM- and 64QAM-OFDM over the vehicular channel.

First, the performance of the QPSK-OFDM system are considered in Figure 25. In this figure, the performance with perfect estimation is lower than the performance over the AWGN channel. The curves for $N_f = 8$ and $N_f = 12$ are very close. Figure 25 also shows that the difference between the perfect estimation curve and the interpolation curves is constant at about 2 dB for spline interpolation and 2.1 dB for lowpass FIR interpolation. A very small performance difference between the lowpass FIR interpolation and the spline interpolation curves can also be observed. The difference is about 0.3 dB at a BER of 10^{-3}. The curves for 16QAM-, and 64QAM-OFDM also show similar performance differences between the perfect estimation and the interpolation curves. Consider a BER of 10^{-3} with lowpass FIR interpolation and $N_f = 8$. From Figures 25, 26, and 27, one can observe that the QPSK-, 16QAM-, and 64QAM-OFDM systems require a value of E_b/N_0 of about 21.7 dB, 24 dB, and 28 dB, respectively. The vehicular channel is a much more severe channel. Therefore, system performance is lower than for the indoor to outdoor/pedestrian channel.

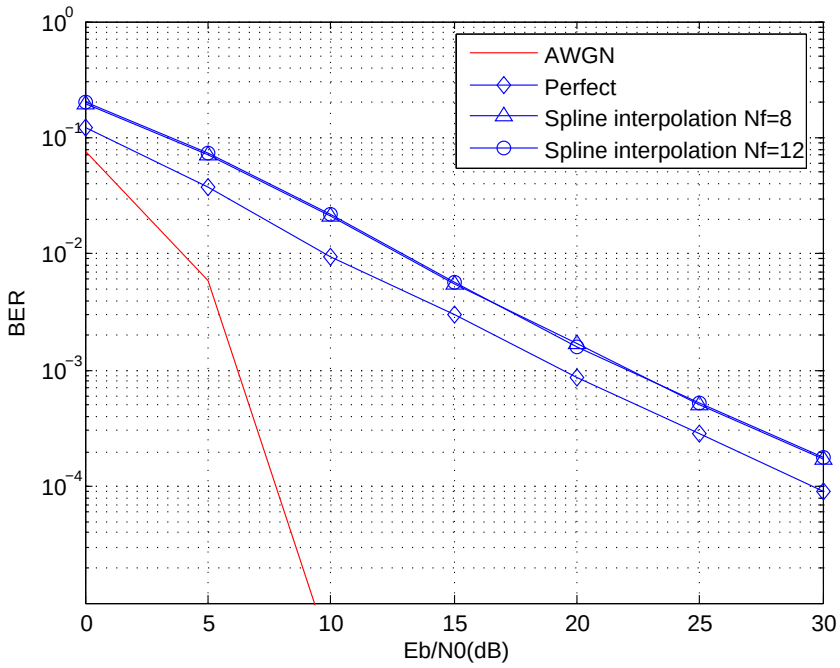

(a) Spline interpolation.

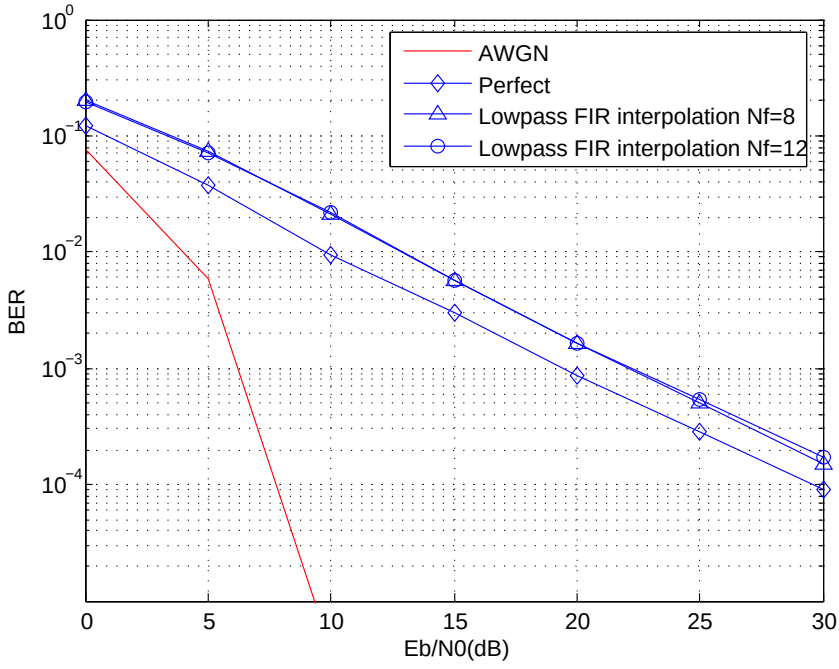

(b) Lowpass FIR interpolation.

Figure 25: *Performance of the QPSK-OFDM system over the vehicular channel.*

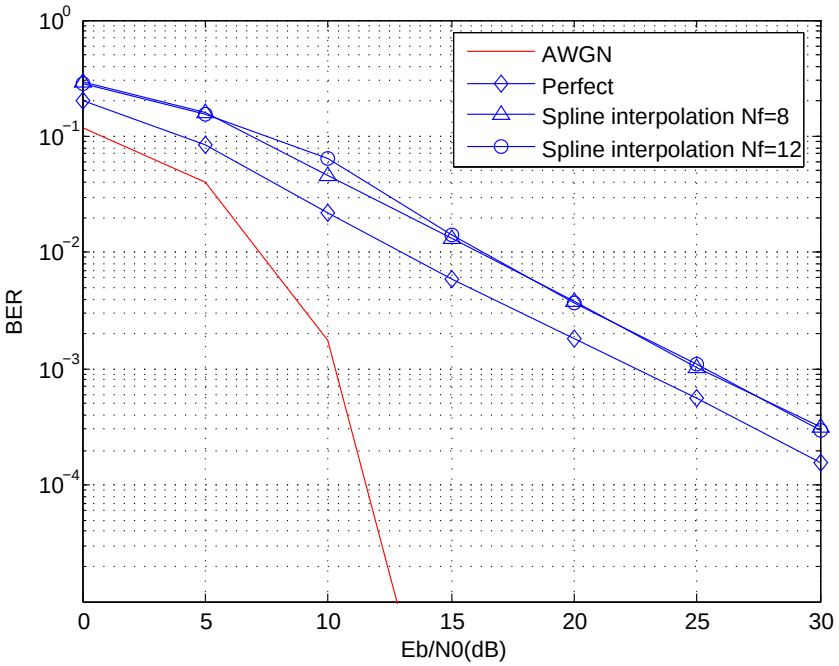

(a) Spline interpolation.

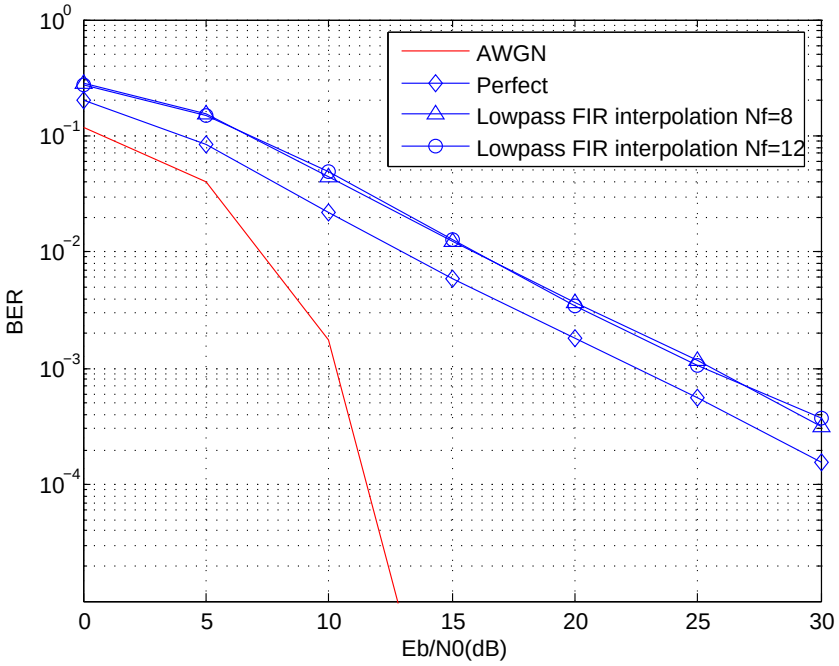

(b) Lowpass FIR interpolation.

Figure 26: *Performance of the 16QAM-OFDM system over the vehicular channel.*

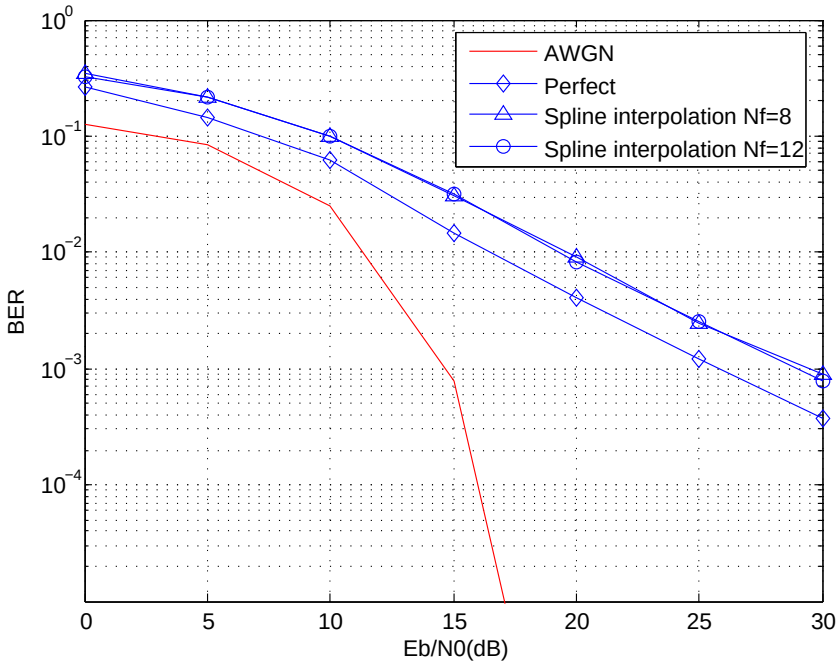

(a) Spline interpolation.

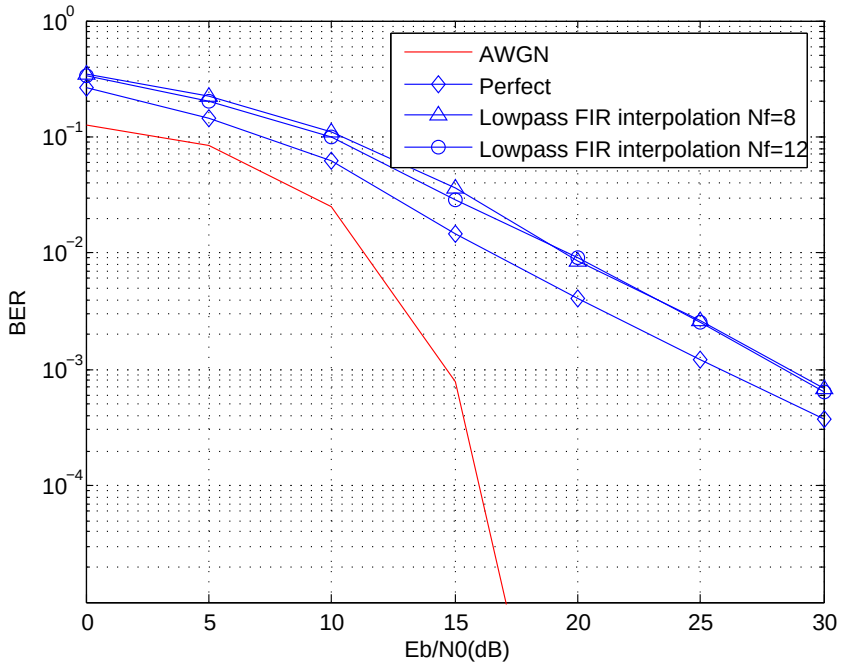

(b) Lowpass FIR interpolation.

Figure 27: *Performance of the 64QAM-OFDM system over the vehicular channel.*

5.3 OFDM simulation results summary

In this section, a simple AWGN channel was used as a benchmark for all BER vs. E_b/N_0 plots. For the AWGN case, the BER diminishes with increasing SNR as expected. Notice that as the Doppler spread f_D increases, the variations of the channel are more rapid. Thus, the channel estimation is better when the channel is not fast varying (indoor to outdoor/pedestrian). This leads to better performance than for the vehicular environment. Also, if the period of the pilot tones is small, the estimation is more accurate, as can be seen, when the performance with $N_f = 8$ and $N_f = 12$ are compared. When the channel varies faster, the pilot tone insertion rate need to be increased to get better estimates of the channel. The performance of OFDM over the indoor to outdoor channel is better than over the vehicular channel. In fact, coding techniques will probably have to be used in order to improve the performance of the system for the vehicular channel.

6 MC-CDMA simulation parameters

As mentioned in a section 2.3, MC-CDMA is a combination of OFDM and CDMA. Such a combination has the benefits of both OFDM and CDMA. In MC-CDMA, symbols are modulated on several subcarriers to introduce frequency diversity instead of using only one carrier like in CDMA. Figures 28 and 29 show MC-CDMA transmitter and receiver configurations for the j^{th} user.

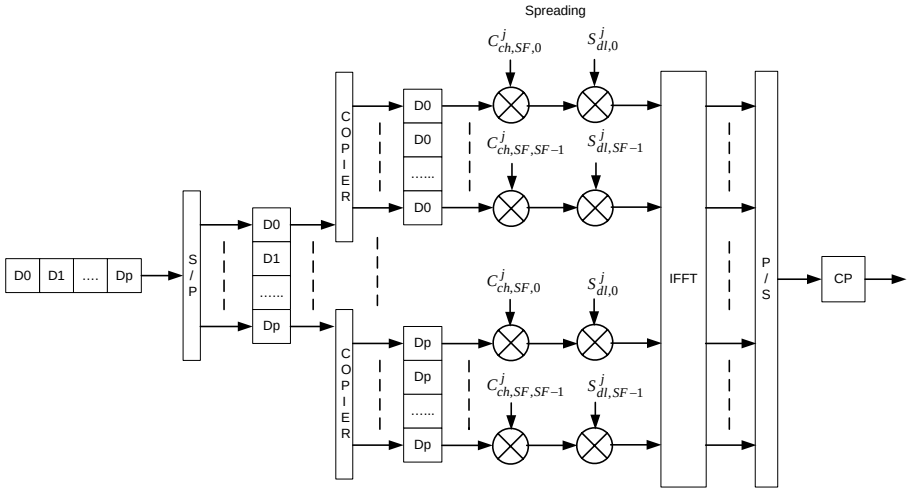

Figure 28: *MC-CDMA transmitter.*

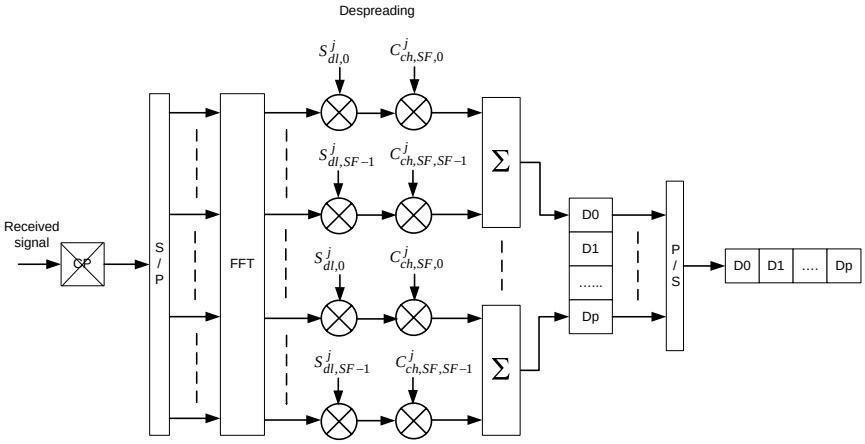

Figure 29: *MC-CDMA receiver.*

$C^j_{ch,SF,k} = [C^j_{ch,SF,0}\ \ C^j_{ch,SF,1}\ \ \cdots\ \ C^j_{ch,SF,SF-1}]$ is the channelisation code, $S^j_{dl,k} = [S^j_{dl,0}\ \ S^j_{dl,1}\ \ \cdots\ \ S^j_{dl,SF-1}]$ is the complex-valued scrambling code of the j^{th} user in

the frequency domain, and SF denotes the spreading factor of the code. As shown in Figure 28, the modulated data symbol sequence is serial-to-parallel converted to N parallel sequences (i.e. N is equal to the number of data subcarriers and the number of pilot subcarriers, see section 4). Each of the parallel sequences is duplicated into SF parallel copies and each of the duplicated symbols is multiplied by a chip from the spreading code, which is the combination of a chip from the channelisation code and a chip from the scrambling code. Finally, an IFFT is performed and a guard interval is inserted to generate the MC-CDMA signal.

In WCDMA, the scrambling codes are used to identify cells (base station), and the channelisation codes are Orthogonal Variable Spreading Factor (OVSF) codes that are used to separate downlink connections to different users within one cell as shown in Figure 30. In the uplink, scrambling codes are used to identify mobiles, and channelisation codes are used to identify physical channels from the same mobile, (i.e. to preserve the orthogonality between a user's different physical channels such as Dedicated Physical Data Channel (DPDCH) and Dedicated Physical Control Channel (DPCCH) from the same mobile user [15]) as shown in Figure 31.

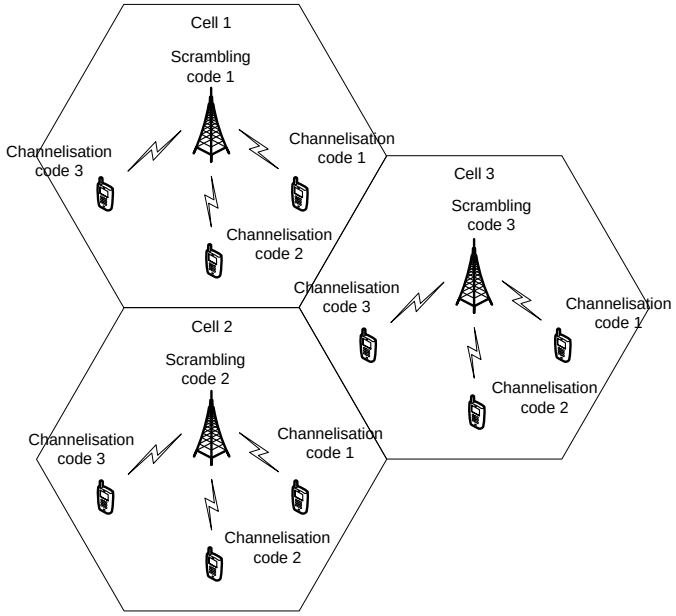

Figure 30: *Spreading code function in downlink.*

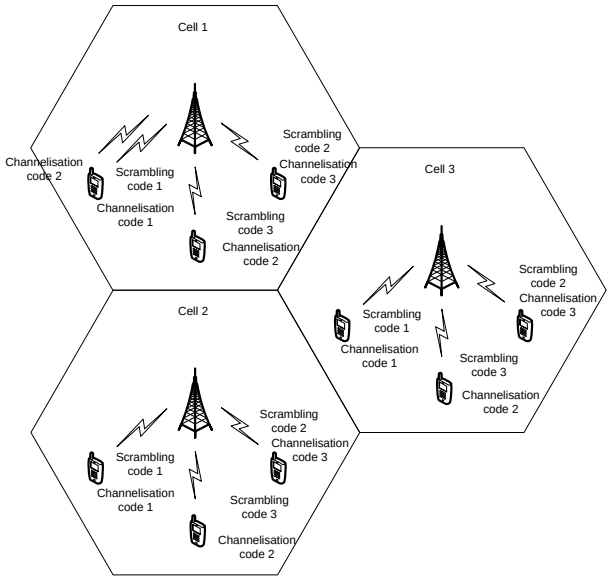

Figure 31: *Spreading code function in uplink.*

One can see that in the downlink, a base station uses only a single scrambling code and several channelisation codes. Meanwhile, in the uplink, all mobile have different scrambling codes for separating users. The downlink spreading in WCDMA is illustrated in Figure 32 [15]. In this figure, the I and Q branches are spread by the same real-valued channelisation codes which are uniquely described as $C^{j}_{ch,SF,k}$ in Figure 33, where k is the code number, $0 \leq k \leq SF - 1$. Then, the sequence of chips is scrambled (complex chip-wise multiplication) by a complex-valued scrambling code $S_{dl,k}$. The scrambling codes in the downlink direction use Gold codes which are constructed by combining two real sequences into a complex-valued sequence. In the WCDMA downlink, the scrambling codes are constructed by using polynomials $1 + X^7 + X^{18}$ and $1 + X^5 + X^7 + X^{10} + X^{18}$ as shown in Figure 34 [15].

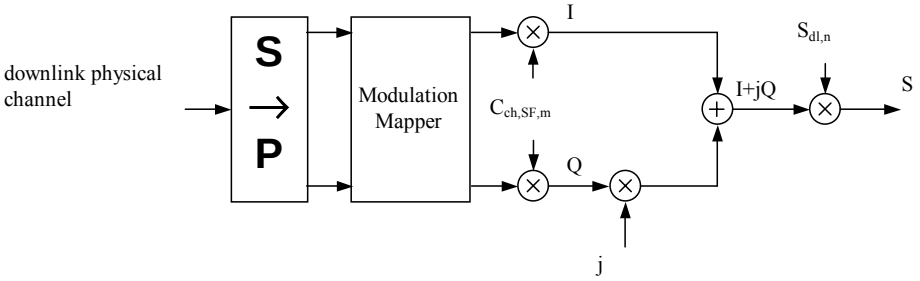

Figure 32: *Spreading for a downlink physical channel.*

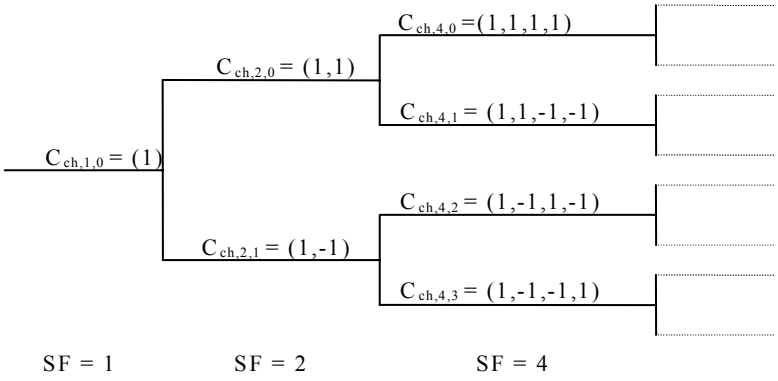

Figure 33: *Code-tree for generation of the OVSF codes.*

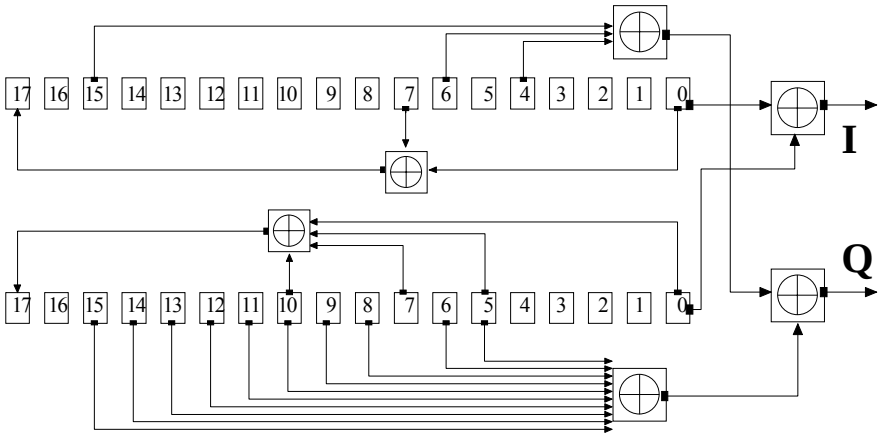

Figure 34: *Downlink scrambling code generator.*

6.1 Indoor to outdoor/pedestrian channel

In section 4, the simulation parameters for the OFDM systems have been calculated. These parameters were used to calculate the simulation parameters for the MC-CDMA systems. As mentionned in the OFDM simulation section, the FFT length of the OFDM system is equal to 64. In this section, the spreading factor is assumed to be $SF = 8$, leading to an FFT length for the MC-CDMA system equal to 512. For simplicity, the MC-CDMA system uses only channelisation codes for the spreading operation. Given a channel bandwidth $BW = 5$ MHz and a sampling rate of $F_s = 5$ MHz, the subcarrier spacing of the MC-CDMA system is

$$\Delta f = \frac{F_s}{N_{FFT}} = \frac{5 \times 10^3}{512} = 9.765625 \text{ kHz} \tag{36}$$

Effective symbol duration (FFT interval duration):

$$T = \frac{1}{\Delta f} = 102.4 \ \mu\text{s} \tag{37}$$

Guard interval:

$$GI = \frac{T}{4} = 25.6 \ \mu\text{s} \tag{38}$$

MC-CDMA symbol duration:

$$T_S = T + GI = 102.4 \ \mu\text{s} + 25.6 \ \mu\text{s} = 128 \ \mu\text{s} \tag{39}$$

Pilot tone spacing:

$$N_f \leq \frac{0.5}{\tau_{max} \Delta f} = \frac{0.5}{488 \times 10^{-9} \times 9.765625 \times 10^3} \approx 105 \tag{40}$$

As mentioned in section 4, the symbol rate is equal to the total number of subcarriers divided by the OFDM symbol duration. The MC-CDMA symbol rate is also equal to the total number of subcarriers divided by the MC-CDMA symbol duration. Due to insertion of pilot tones and a spreading factor of SF, the actual symbol rate can be expressed as

$$R_s = \frac{N_C}{T_S \times SF} \tag{41}$$

where N_C is the number of data subcarriers. Then, the maximum bit rate is

$$R_b = R_s \times \log_2 M \tag{42}$$

where $M = \{4, 16, 64\}$ is the constellation size of the modulation. Table 6 shows the simulation parameters for the MC-CDMA system over the indoor to outdoor environment with pilot tone spacings of $N_f = 64$ and $N_f = 94$. The data rate of the MC-CDMA system is around 8 times less than the OFDM system. However, the MC-CDMA system can support up to 8 users compared with the OFDM system which can support only one user. Table 7 shows the bandwidth efficiency for the MC-CDMA system for this channel.

Table 6: *Simulation parameters for the indoor to outdoor/pedestrian environment.*

Available bandwidth	5 MHz	
FFT sampling rate	5 MHz	
Spreading factor	8	
Spreading codes	OVSF codes	
FFT size	512	
Subcarrier spacing	9.765625 kHz	
Effective symbol duration	102.4 μs	
Guard time duration	25.6 μs	
MC-CDMA symbol duration	128 μs	
Pilot spacing	64	94
Number of pilot subcarriers	8	6
Number of data subcarriers	440	464
Number of subcarriers	448	470
Occupied bandwidth	4.38 MHz	4.59 MHz
Actual symbol rate	429.6875 kSps	453.125 kSps

Table 7: *Bandwidth efficiency of MC-CDMA system for the indoor to outdoor environment.*

Pilot spacing	64	94
QPSK	859.375 kbps 0.196 bits/s/Hz	906.25 kbps 0.197 bits/s/Hz
16QAM	1718.75 kbps 0.391 bits/s/Hz	1812.5 kbps 0.394 bits/s/Hz
64QAM	2578.125 kbps 0.587 bits/s/Hz	2718.75 kbps 0.591 bits/s/Hz

6.2 Vehicular channel

The FFT length of the MC-CDMA system in this case is equal to $256 \times 8 = 2048$ and the other parameters can be calculated as follows.

Subcarrier spacing:

$$\Delta f = \frac{F_s}{N_{FFT}} = \frac{5 \times 10^3}{2048} = 2.4414 \text{ kHz} \tag{43}$$

Effective symbol duration (FFT interval duration):

$$T = \frac{1}{\Delta f} = 409.6 \ \mu\text{s} \tag{44}$$

Guard interval:

$$GI = \frac{T}{4} = 102.4 \ \mu\text{s} \tag{45}$$

MC-CDMA symbol duration:

$$T_S = T + GI = 409.2 \ \mu\text{s} + 102.4 \ \mu\text{s} = 512 \ \mu\text{s} \tag{46}$$

Pilot tone spacing:

$$N_f \leq \frac{0.5}{\tau_{max} \Delta f} = \frac{0.5}{1.708 \times 10^{-6} \times 2.4414 \times 10^3} \approx 120 \tag{47}$$

Table 8 shows the simulation parameters for the MC-CDMA system over the vehicular environment with pilot tones spacings of $N_f = 64$ and $N_f = 94$. The maximum data rate of one user is also around 8 times less than for the OFDM system. Table 9 shows the bandwidth efficiency for the MC-CDMA system for this channel.

Table 8: *Simulation parameters for the vehicular environment.*

Available bandwidth	5 MHz	
FFT sampling rate	5 MHz	
Spreading codes	OVSF codes	
FFT size	2048	
Subcarrier spacing	2.4414 kHz	
Effective symbol duration	409.6 μs	
Guard time duration	102.4 μs	
MC-CDMA symbol duration	512 μs	
Pilot spacing	64	94
Number of pilot subcarriers	32	22
Number of data subcarriers	1952	1952
Number of subcarriers	1984	1974
Occupied bandwidth	4.85 MHz	4.77 MHz
Actual symbol rate	476.5625 kSps	476.5625 kSps

Table 9: *Bandwidth efficiency of MC-CDMA system for the vehicular environment.*

Pilot spacing	64	94
QPSK	953.125 kbps 0.196 bits/s/Hz	953.125 kbps 0.2 bits/s/Hz
16QAM	1906.25 kbps 0.393 bits/s/Hz	1906.25 kbps 0.4 bits/s/Hz
64QAM	2859.375 kbps 0.59 bits/s/Hz	2859.375 kbps 0.6 bits/s/Hz

7 MC-CDMA simulation

7.1 MC-CDMA simulation model

In this section, in order to validate the performance of the MC-CDMA systems, Monte Carlo simulations were performed to obtain performance results. These systems were simulated over a wireless channel with different numbers of active users (N_u = 1, 4, and 8). As the number of active users was increased, the impact of multiple access interference (MAI) needed to be considered in the simulations. A simulation block diagram for the MC-CDMA system is shown in Figure 35. The simulation parameters for the multipath fading channels and the channel estimation methods which are mentionned in sections 3 and 4 were also used in these simulations. In the simulations, the performance of the MC-CDMA systems was also compared to the matched filter bound (MFB) of a single user MC-CDMA system, as a benchmark. The MFB of a single user MC-CDMA system is defined as a single user MC-CDMA system simulated with perfect channel knowledge and with no ISI or ICI. Strictly speaking, the MFB was obtained by simulating a restricted single user MC-CDMA system that transmits only a single symbol at a time and uses a long enough cyclic prefix to combat the delay spread of the multipath channels. Therefore, this led to a complete elimination of ISI. Furthermore, the orthogonality of the subcarriers was maintained resulting in no ICI.

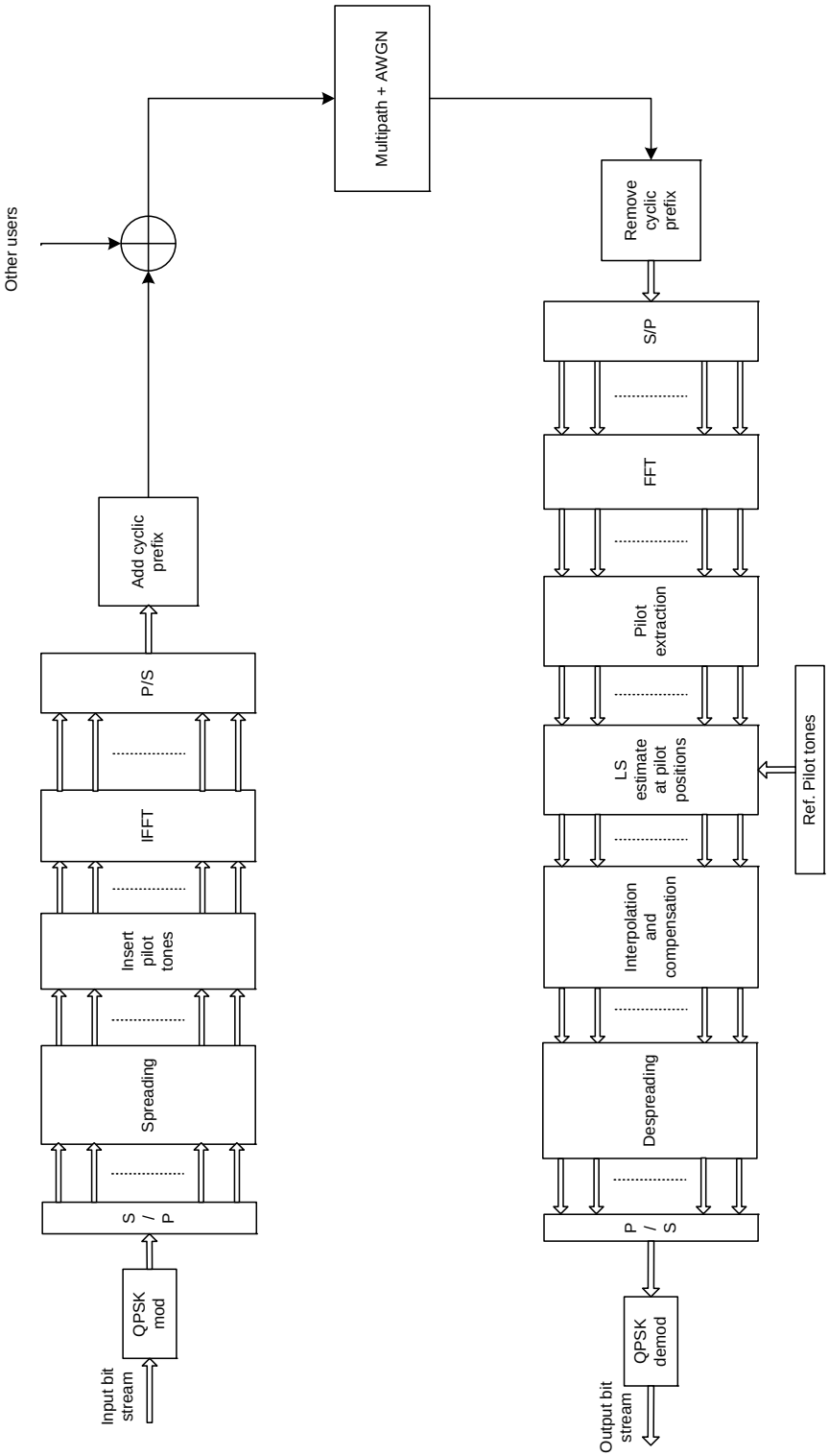

Figure 35: *Simulation block diagram for the MC-CDMA.*

7.2 MC-CDMA simulation results

7.2.1 Number of subcarrier impact

First, the influence of the number of subcarriers on the performance of MC-CDMA systems was considered. Figure 36 illustrates the influence of the number of subcarriers on the performance of QPSK-MC-CDMA over the worst case channel (vehicular channel). The system with 2048 subcarriers had a performance improvement of about 6 dB over the system with 64 subcarriers at a BER of 10^{-3}.

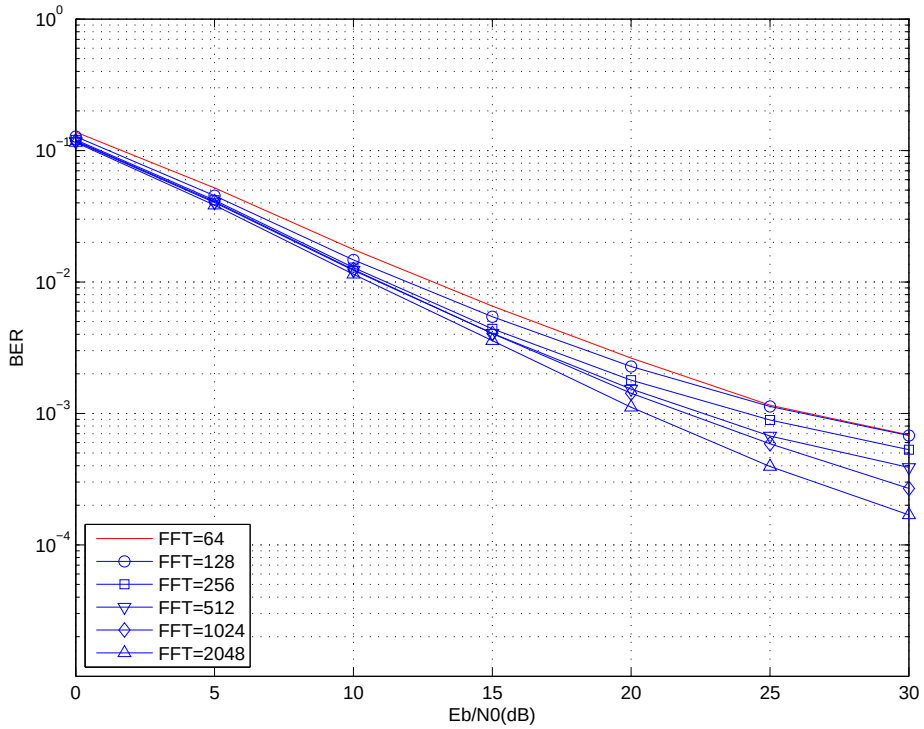

Figure 36: *Influence of the number of subcarriers on the performance of QPSK-MC-CDMA.*

Figure 37 shows the bit error rate performance as a function of the number of subcarriers at $E_b/N_0 = 30$ dB. The more the number of subcarriers is increased, the better the performance is. Since the subcarrier spacing is inversely proportional to the number of subcarriers, the spectrum around each subcarrier is flatter and leads to better performance.

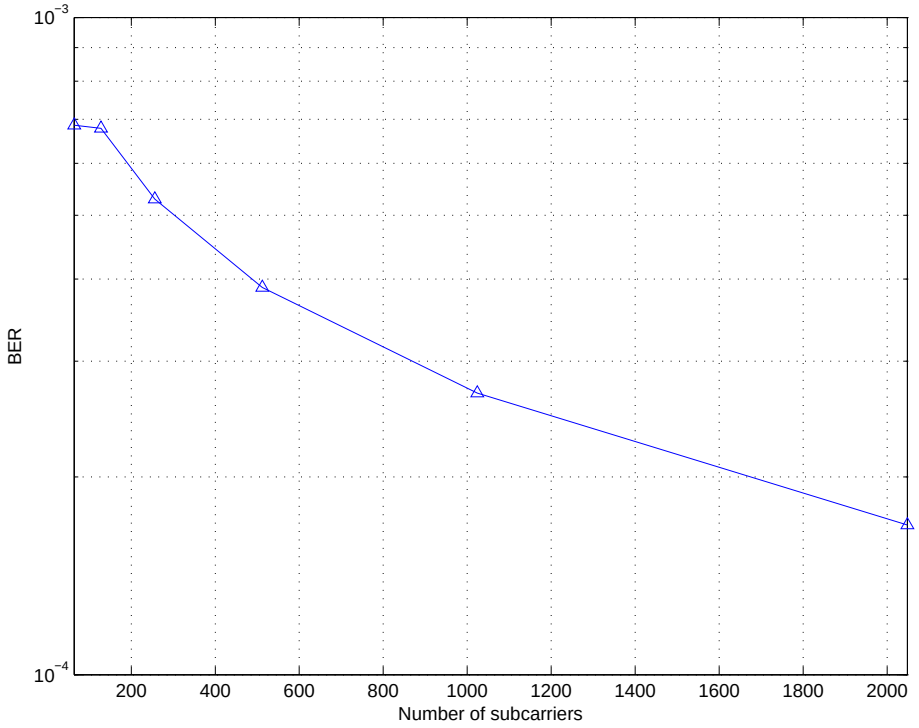

Figure 37: *Influence of the number of subcarriers on the performance of QPSK-MC-CDMA at* $E_b/N_0 = 30$ *dB.*

7.2.2 Results for indoor to outdoor/pedestrian channel

Figures 38 to 43 show the bit error probability as a function of the signal-to-noise ratio for the QPSK-, 16QAM- and 64QAM-MC-CDMA systems over the indoor to outdoor channel with the number of users equal to $N_u = 1$, 4, and 8. The channel estimation uses the spline interpolation and lowpass FIR interpolation methods with different pilot tone spacings. In these figures, the same representation of the curves for two sets of figures was used, one for the spline and another for lowpass FIR interpolation. The solid curves represent the performances for the matched filter bound (MFB) in a single user MC-CDMA system. The solid curves with diamond markers represent performance of the system using perfect knowledge of the channel. The solid curves with circle markers represent performance of the system with $N_u = 1$. The solid curves with square markers represent performance of the system with $N_u = 4$. Finally, the solid curves with downward-pointing triangle markers represent performance of the system with $N_u = 8$.

First, the performance of the QPSK-MC-CDMA system in Figures 38, and 39 was considered. In these figures, there is a small gap between the perfect curves and

the MFB curves. The gap is about 0.7 dB at a BER of 10^{-3}. The MFB curves show better performances as expected. This is because the MFB was simulated with better conditions (perfect channel knowledge and with no ISI or ICI). Since the lowpass FIR interpolation method will be used for hardware implementations, only the performance of this method was considered. For the desired user only, $N_u = 1$, these figures show the difference between the perfect and the interpolation curves to be constant at about 2.7 dB for both $N_f = 64$ and $N_f = 94$ at a BER of 10^{-3}. For $N_u = 4$ users, the difference between the perfect and the interpolation curves is also constant at about 7 dB for both $N_f = 64$ and $N_f = 94$. The difference is about 9.2 dB when the number of users is $N_u = 8$. The performance of the desired user is degraded as the number of interferers is increased. This is because the interferers can be treated as additive noise to the desired user. For example in Figure 38, the performance degradation of the system with 3 interferers ($N_u = 4$, i.e. 50% user load) is about 4.3 dB as compare with approximately 6.5 dB with 7 interferers (i.e. 100% user load) at a BER of 10^{-3}. The curves for the 16QAM-, and 64QAM-MC-CDMA also show similar performance differences with different numbers of active users. From Figures 40 and 42, the performance degradation of the system with 3 interferers ($N_u = 4$, i.e. 50% user load) is about 5 dB and 6 dB for 16QAM-, and 64QAM-MC-CDMA, respectively, as compare with approximately 7.6 dB and 8 dB for 16QAM-, and 64QAM-MC-CDMA, respectively, with 7 interferers (i.e. 100% user load) at a BER of 10^{-3}. The influence of pilot tone spacing on the performance of the systems is very small. This is because pilot tone spacing satisfies the Sampling Theorem [9].

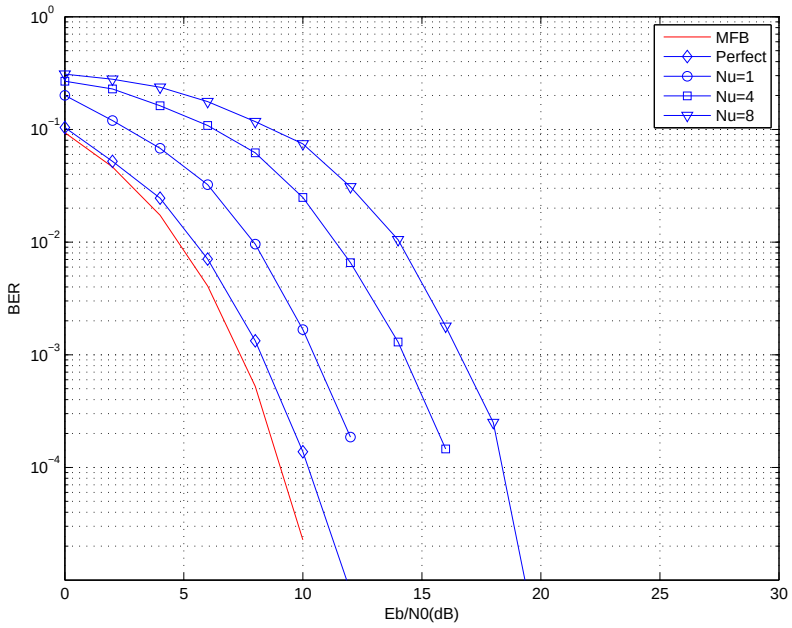

(a) Spline interpolation.

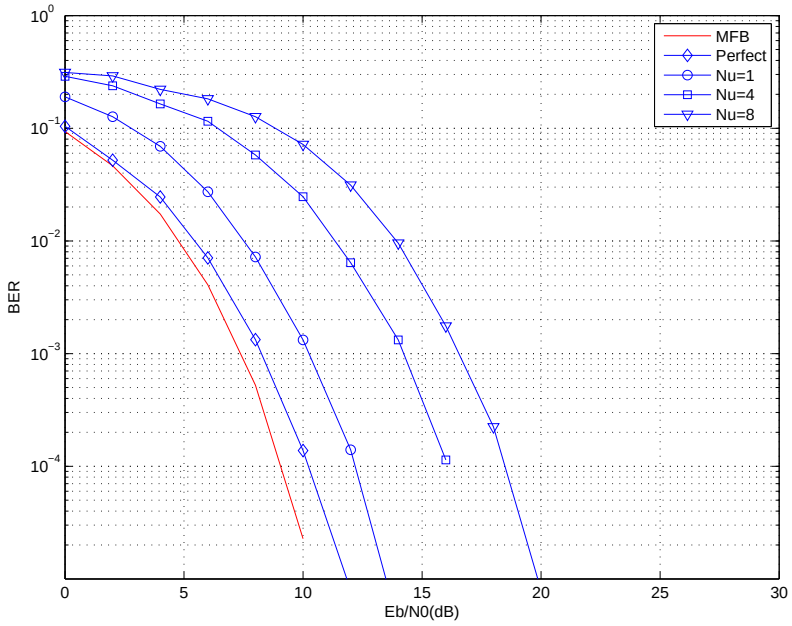

(b) Lowpass FIR interpolation.

Figure 38: *Performance of the QPSK-MC-CDMA system over the indoor to outdoor channel,* $N_f = 64$.

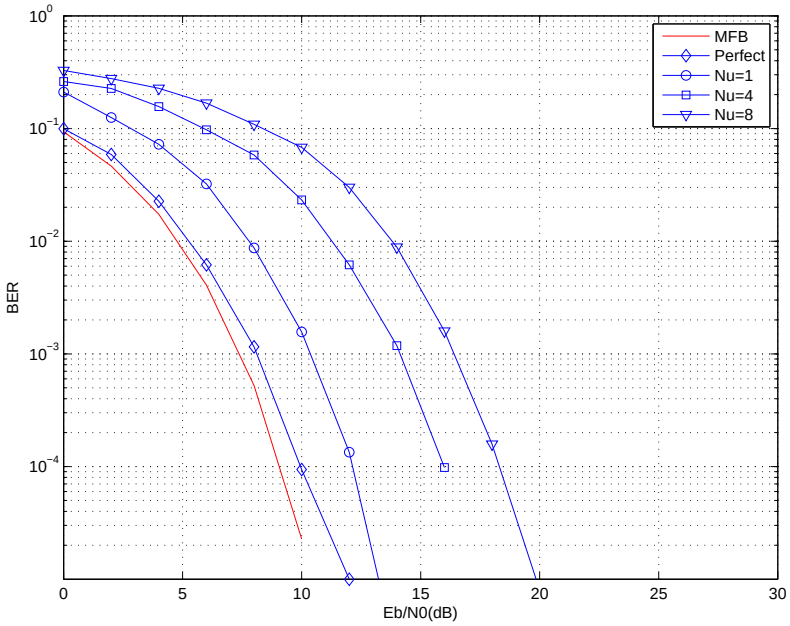

(a) Spline interpolation.

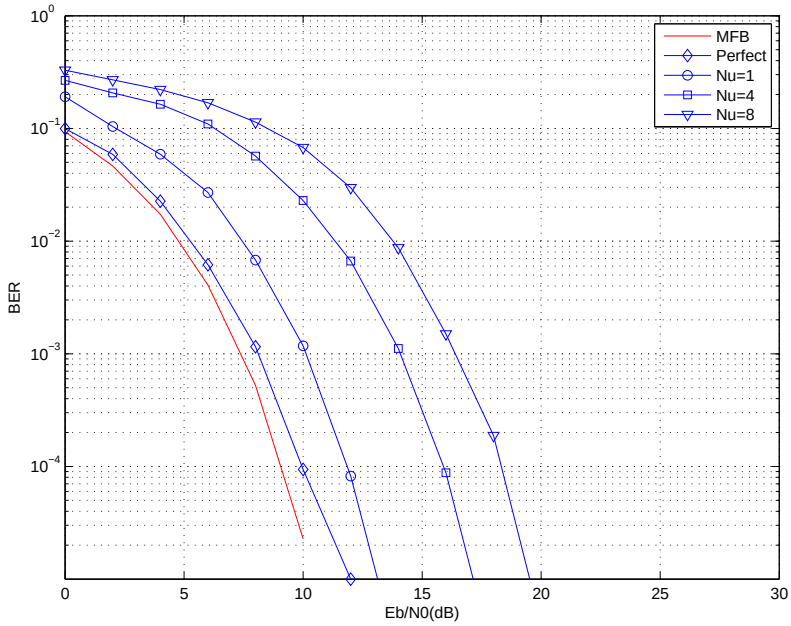

(b) Lowpass FIR interpolation.

Figure 39: *Performance of the QPSK-MC-CDMA system over the indoor to outdoor channel,* $N_f = 94$.

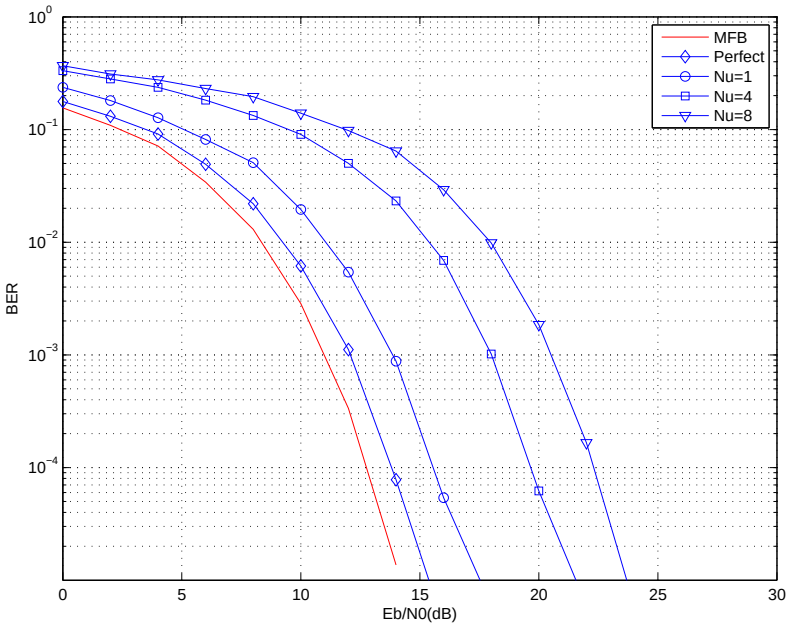

(a) Spline interpolation.

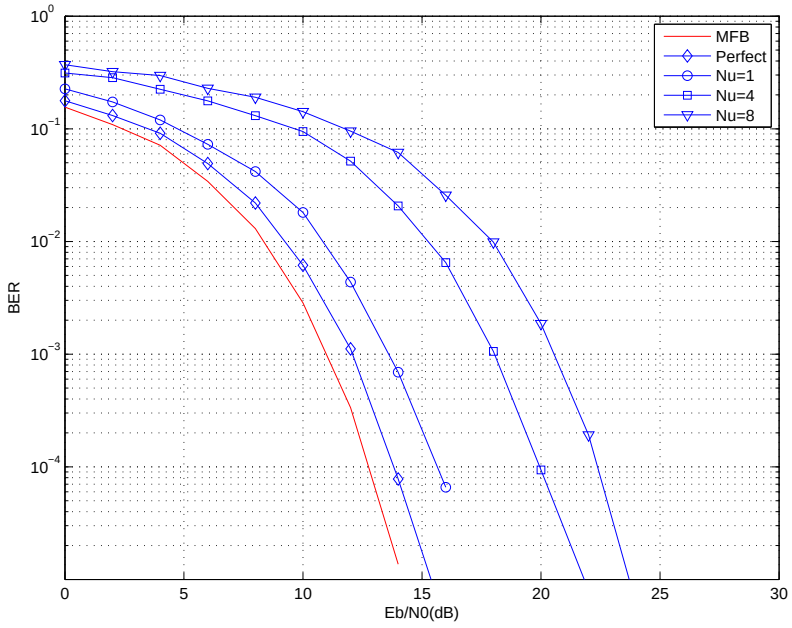

(b) Lowpass FIR interpolation.

Figure 40: *Performance of the 16QAM-MC-CDMA system over the indoor to outdoor channel,* $N_f = 64$.

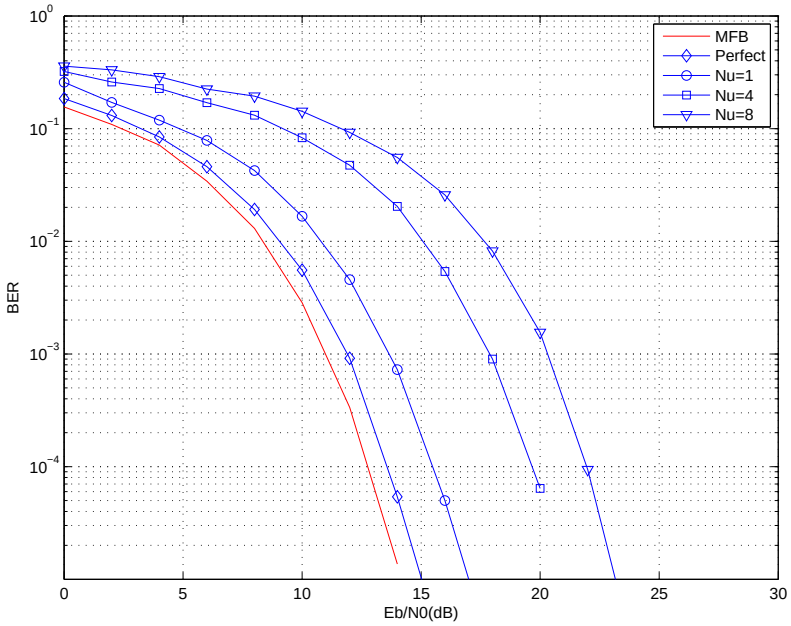

(a) Spline interpolation.

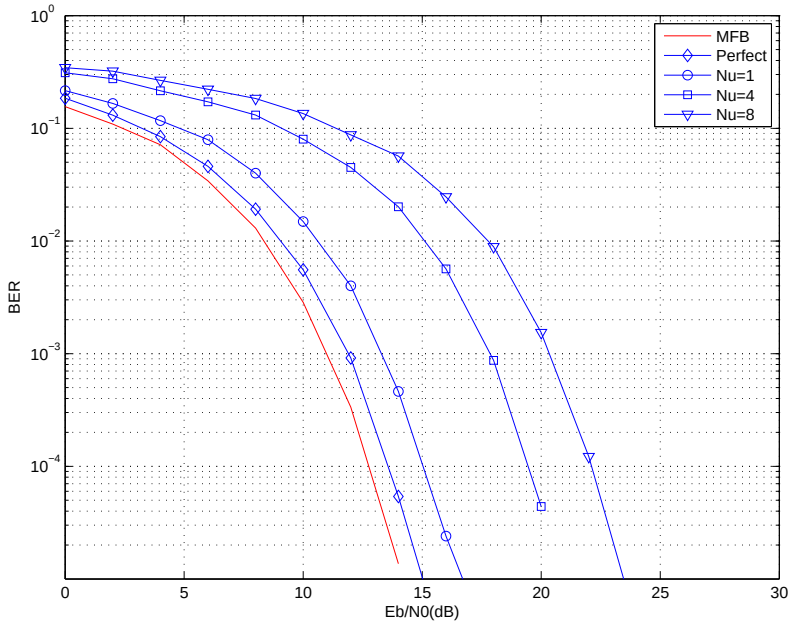

(b) Lowpass FIR interpolation.

Figure 41: *Performance of the 16QAM-MC-CDMA system over the indoor to outdoor channel,* $N_f = 94$.

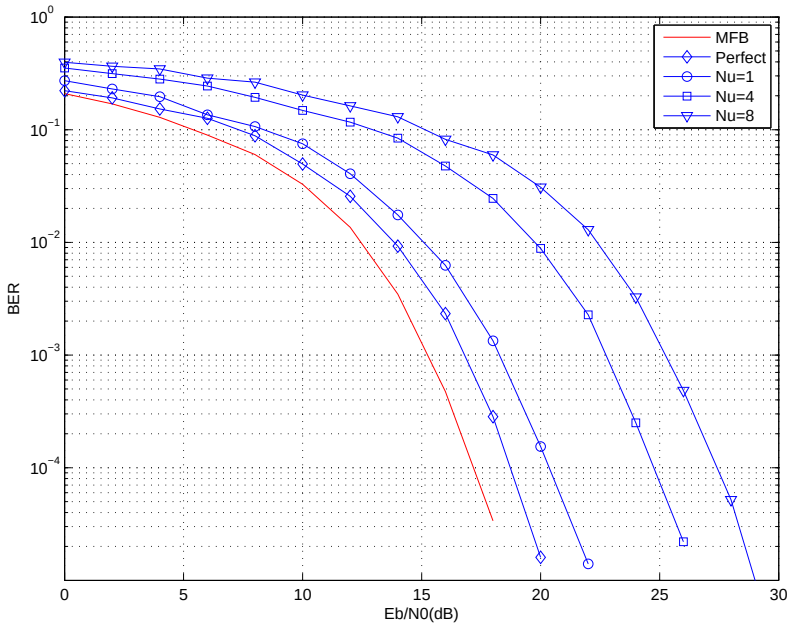

(a) Spline interpolation.

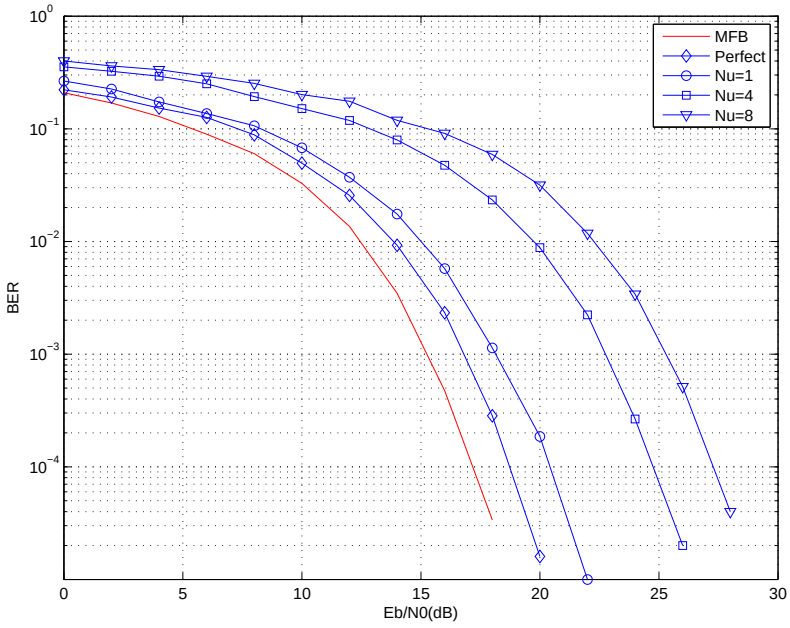

(b) Lowpass FIR interpolation.

Figure 42: *Performance of the 64QAM-MC-CDMA system over the indoor to outdoor channel,* $N_f = 64$.

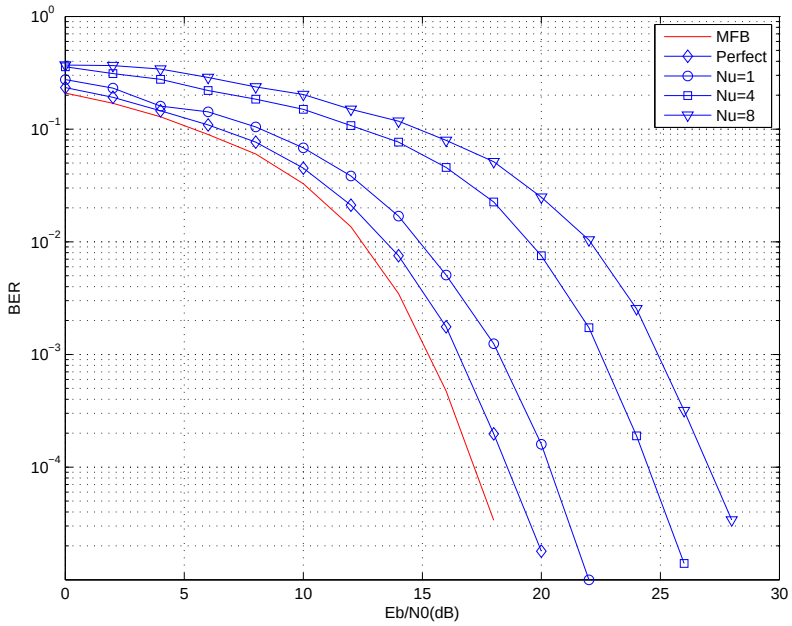

(a) Spline interpolation.

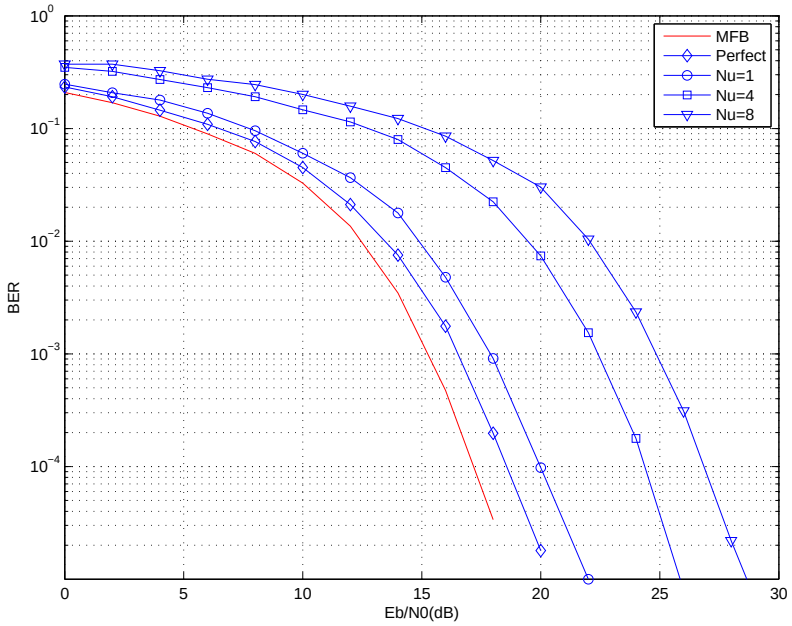

(b) Lowpass FIR interpolation.

Figure 43: *Performance of the 64QAM-MC-CDMA system over the indoor to outdoor channel,* $N_f = 94$.

7.2.3 Results for vehicular channel

Figures 44 to 49 show the performance of QPSK-, 16QAM- and 64QAM-MC-CDMA systems over the vehicular channel using the same simulation parameters as for the indoor to outdoor channel, with different numbers of users ($N_u = 1, 4$, and 8).

In Figures 44 and 45, there is a small gap between the perfect and the MFB curves. The gap is about 1.7 dB at a BER of 10^{-3}. Again, the performance of the desired user is degraded as the number of interferers increases. Furthermore, the performance of the system over the vehicular channel is lower than those over the indoor to outdoor/pedestrian channel. This is because the vehicular channel is a much more severe environment than the indoor to outdoor environment. For example, in Figures 44 and 45, the performance degradation of the QPSK-MC-CDMA system with 3 interferers ($N_u = 4$, i.e. 50% user load) is about 3.8 dB as compare with approximately 6.3 dB with 7 interferers (i.e. 100% user load) at a BER of 10^{-3}. The curves for 16QAM-, and 64QAM-MC-CDMA also show similar performance differences with different numbers of active users. From Figures 46 and 48, the performance degradation of the system with 3 interferers ($N_u = 4$, i.e. 50% user load) is about 4.7 dB and 5.7 dB for 16QAM-, and 64QAM-MC-CDMA, respectively, as compare with approximately 7.7 dB and 8 dB for 16QAM-, and 64QAM-MC-CDMA, respectively, with 7 interferers (i.e. 100% user load) at a BER of 10^{-3}. Again, for the same reason as in the previous section, the influence of pilot tone spacing on the performance of the systems is very small.

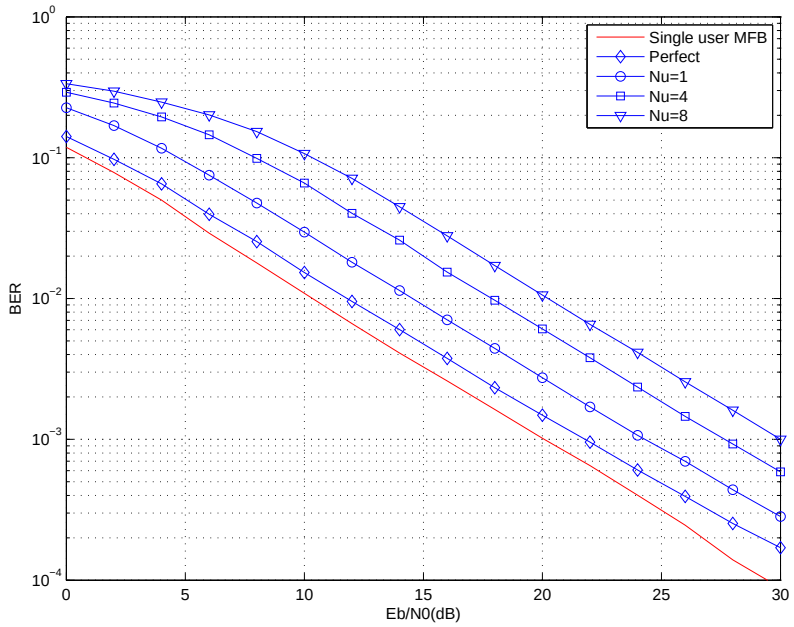

(a) Spline interpolation.

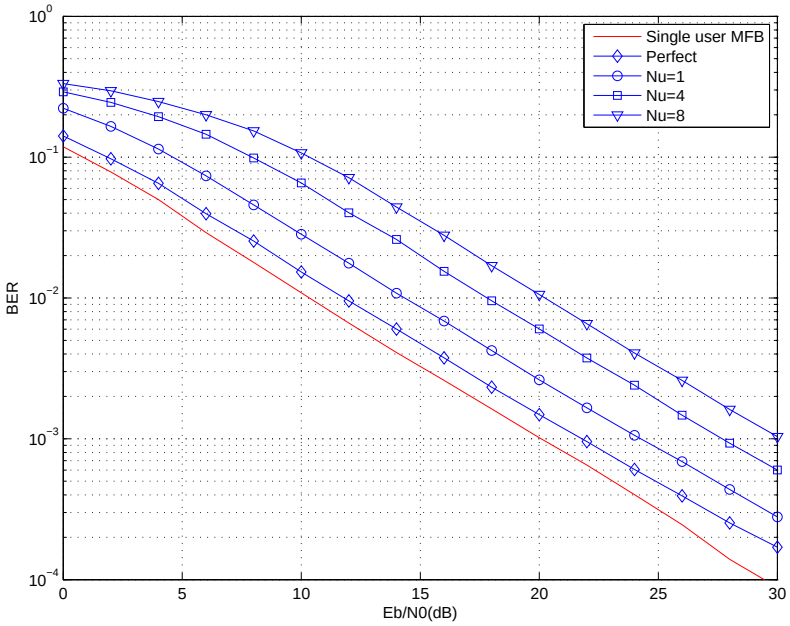

(b) Lowpass FIR interpolation.

Figure 44: *Performance of the QPSK-MC-CDMA system over the vehicular channel,* $N_f = 64$.

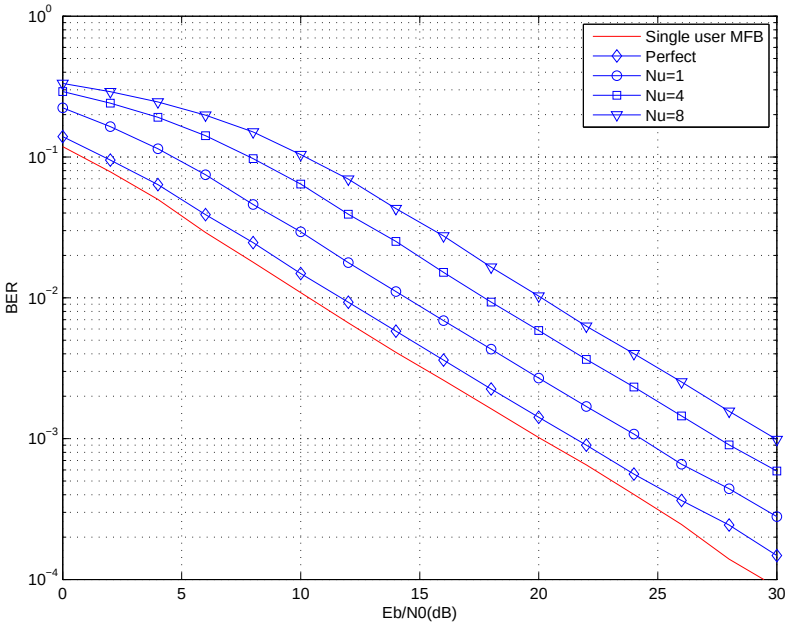

(a) Spline interpolation.

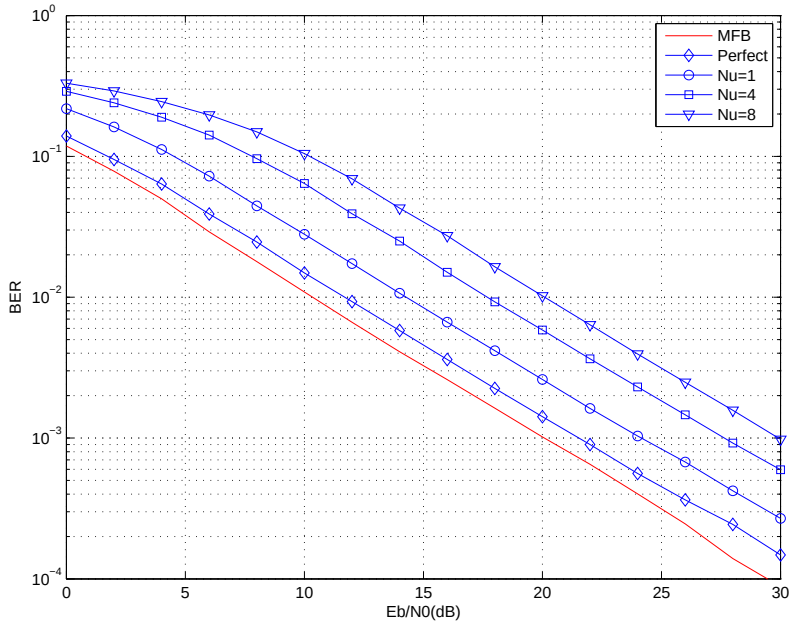

(b) Lowpass FIR interpolation.

Figure 45: *Performance of the QPSK-MC-CDMA system over the vehicular channel,* $N_f = 94$.

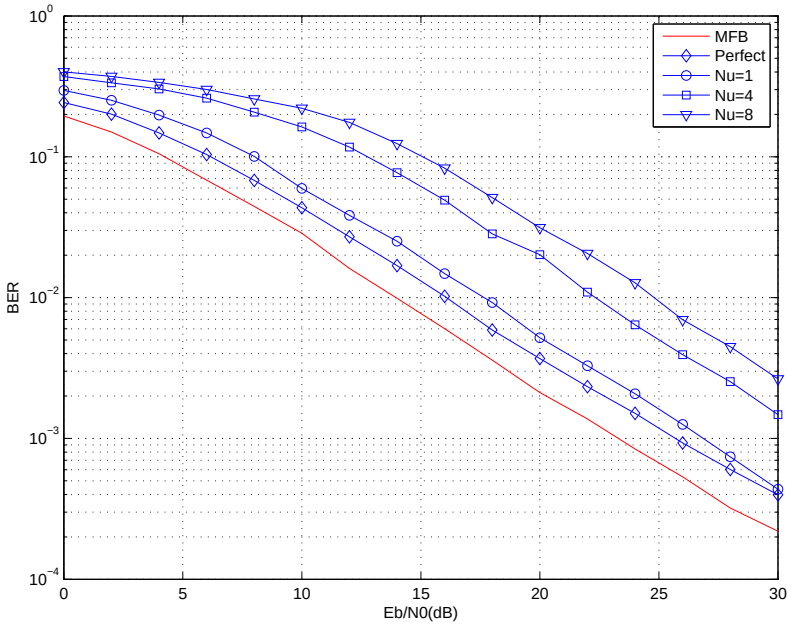

(a) Spline interpolation.

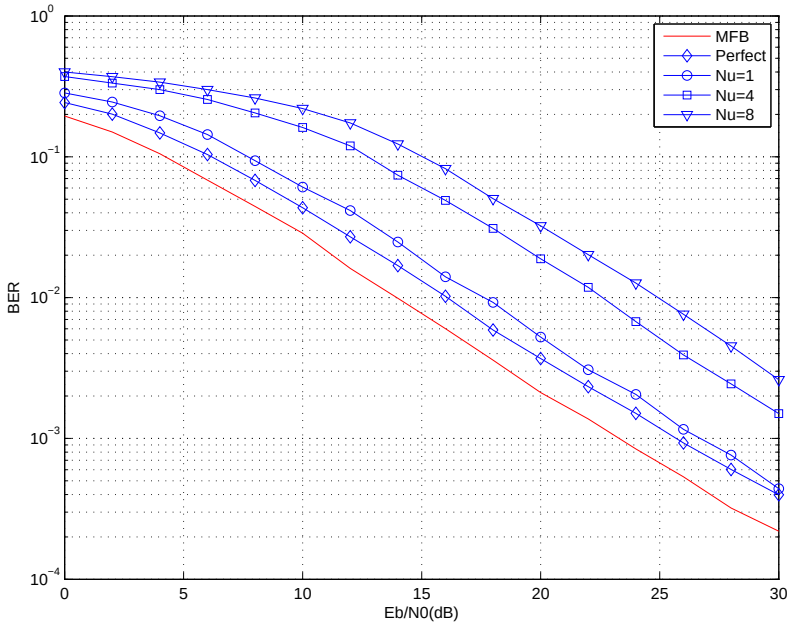

(b) Lowpass FIR interpolation.

Figure 46: *Performance of the 16QAM-MC-CDMA system over the vehicular channel,* $N_f = 64$.

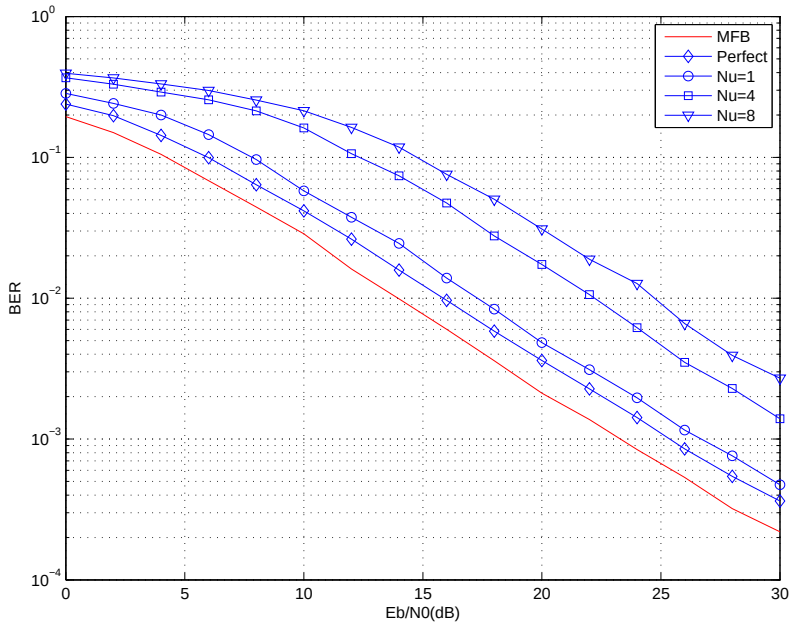

(a) Spline interpolation.

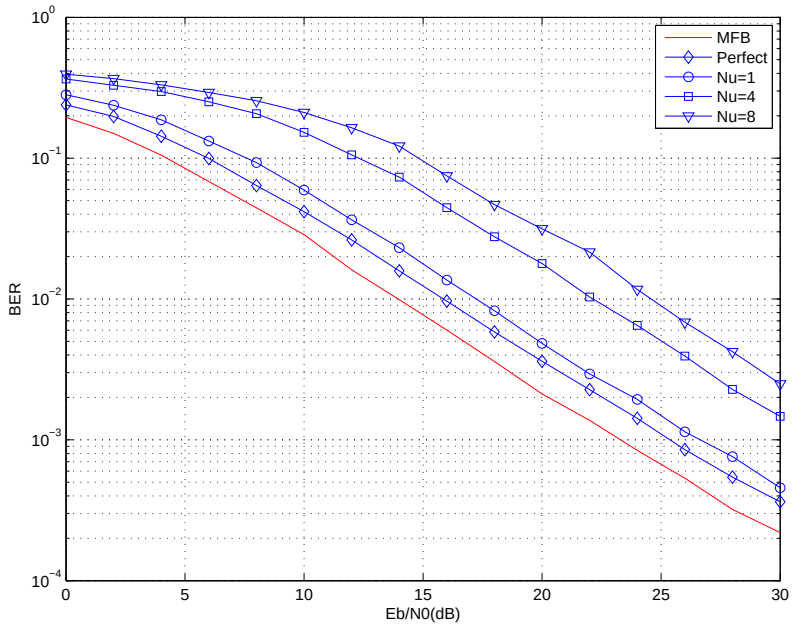

(b) Lowpass FIR interpolation.

Figure 47: *Performance of the 16QAM-MC-CDMA system over the vehicular channel,* $N_f = 94$.

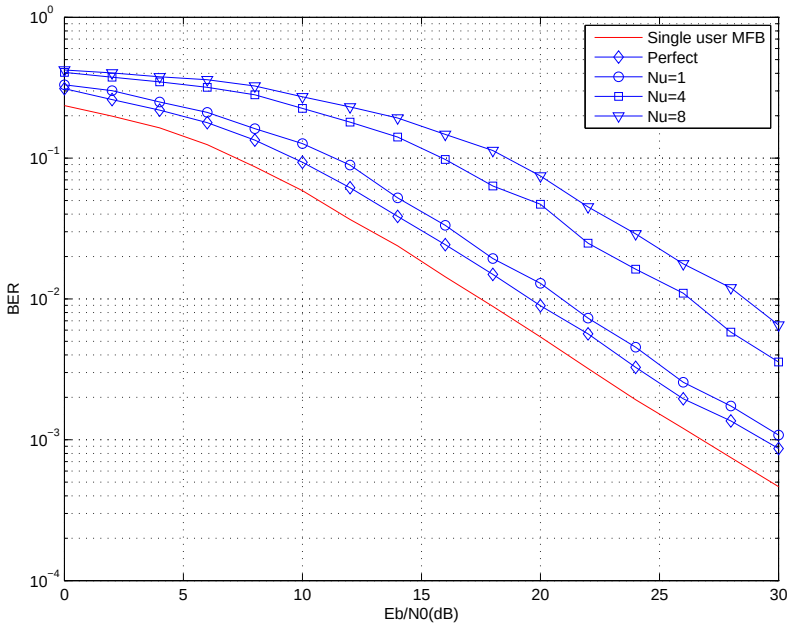

(a) Spline interpolation.

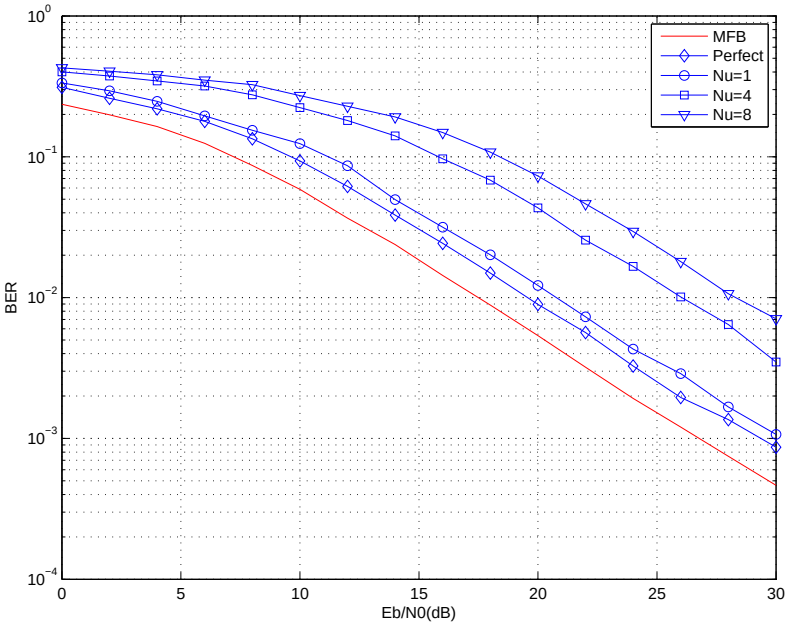

(b) Lowpass FIR interpolation.

Figure 48: *Performance of the 64QAM-MC-CDMA system over the vehicular channel,* $N_f = 64$.

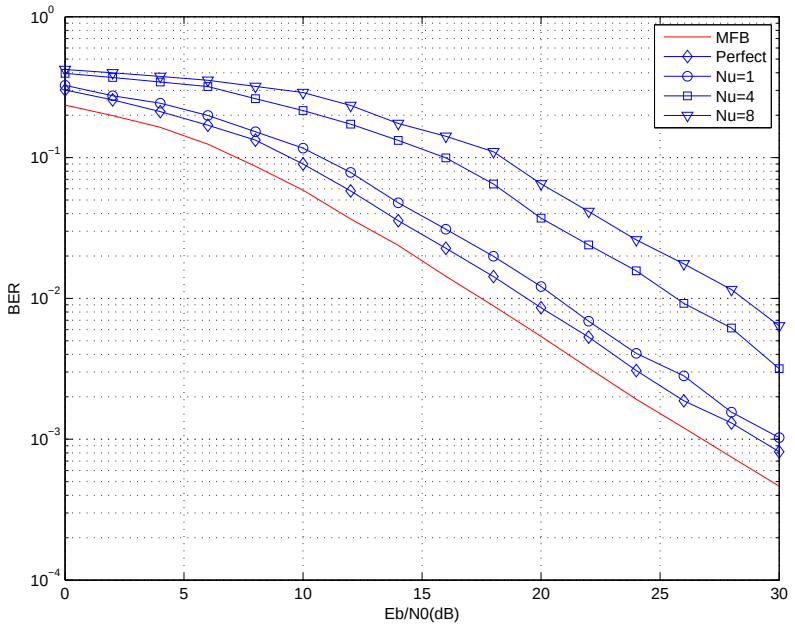

(a) Spline interpolation.

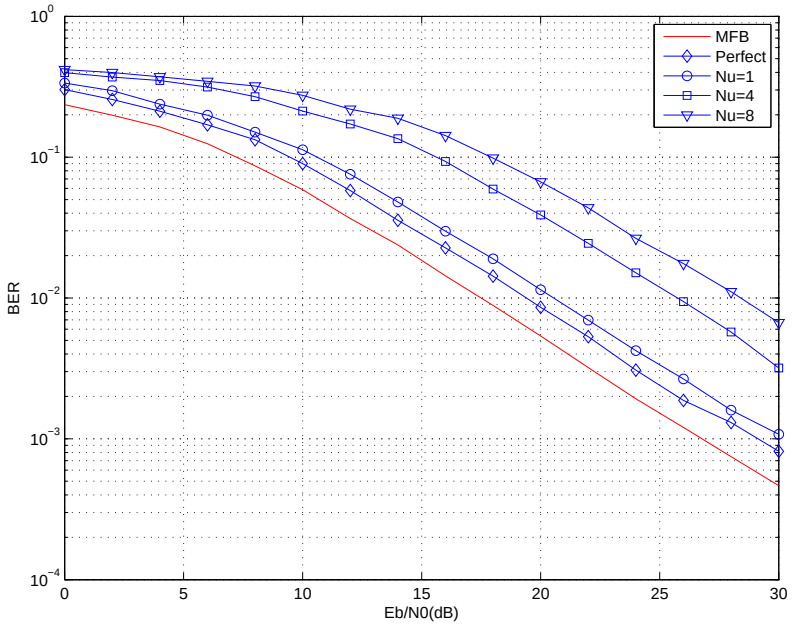

(b) Lowpass FIR interpolation.

Figure 49: *Performance of the 64QAM-MC-CDMA system over the vehicular channel,* $N_f = 94$.

7.3 MC-CDMA simulation results summary

The single user matched filter bound curves were used as a benchmark for all BER vs. E_b/N_0 plots. The BER performance degrades as the number of active users increases (i.e. the BER curves move to the right as the number of users increases). This is due to the impact of interference from other users. As the modulation order increases, a larger bit rate can be transmitted within the same bandwidth, but the BER curves move in the direction of degraded error performance. Given a channel bandwidth of 5 MHz, the MC-CDMA systems can achieve a maximum average data rate of 900 kbps, 1.8 Mbps, and 2.7 Mbps per user for QPSK, 16QAM, and 64QAM, respectively. Table 10 shows a summary of simulation results for MC-CDMA over both indoor to outdoor and vehicular channels with 8 users for a BER of 10^{-3} using the lowpass FIR interpolation method. Similarily, Table 11 shows a summary of simulation results for MC-CDMA over both channels with 8 users for an E_b/N_0 of 15 dB using the lowpass FIR interpolation method.

Table 10: *Performance for both channels with 8 users for a BER of* 10^{-3}.

Modulation	Indoor to outdoor		Vehicular	
Pilot spacing	64	94	64	94
Signal-to-noise ratio	E_b/N_0			
QSPK	11.8 dB	12 dB	30 dB	30 dB
16QAM	21.5 dB	21 dB	-	-
64QAM	25.1 dB	24.9 dB	-	-

Table 11: *Performance for both channels with 8 users for an* E_b/N_0 *of 15 dB.*

Modulation	Indoor to outdoor		Vehicular	
Pilot spacing	64	94	64	94
Bit error rate	BER			
QSPK	3.9×10^{-3}	3.8×10^{-3}	3.4×10^{-2}	3.4×10^{-2}
16QAM	3.9×10^{-2}	3.9×10^{-2}	2.8×10^{-2}	2.8×10^{-2}
64QAM	10^{-1}	10^{-1}	1.4×10^{-1}	1.4×10^{-1}

8 Conclusions

This report presented simulations of a complete Multi-Carrier Code Division Multiple Access (MC-CDMA) system (modulation, transmission over multipath fading channel, reception, and demodulation). The simulation results showed that at a BER of 10^{-3} the performance of the MC-CDMA system over the indoor to outdoor/pedestrian channel is better than for the vehicular channel by about 18 dB, 9 dB, and 6 dB for QPSK-, 16QAM-, and 64QAM-MC-CDMA, respectively. If the channel condition is better, higher modulation orders can be used to improve the transmission data rate. Increasing the modulation order implies that the signal constellation points are closer, leading to a higher BER for the same transmission power. Thus, there has to be a tradeoff between the data rate and the transmission power in order to keep cost low. In fact, coding techniques will have to be used in order to improve the performance of the system for both channels. Turbo codes and Low Density Parity Check (LDPC) codes are the best candidates for performance improvement. Since not much improvement was observed by reducing pilot tone spacing, this parameter could be increased in order to obtain higher bandwidth efficiency at the expense of performance. Matlab was the simulation tool used to implement the MC-CDMA simulation model. This model implementation can be use as a reference tool for future FPGA implementations. Using the model, the right parameters can be found to speedup the FPGA implementation. Multiple-Input Multiple-Output (MIMO) techniques can significantly increase the data rates of wireless systems without increasing channel bandwidth. Therefore, MIMO-MC-CDMA techniques would be worth considering for future investigations.

References

[1] 3GPP (1999). TS 25.101v2.1.0, 3rd Generation Partnership Project (3GPP), Technical Specification Group (TSG), RAN WG4 UE Radio transmission and Reception (FDD).

[2] Hsieh, M.-H. and Wei, C.-H. (1998). Channel estimation for OFDM systems based on comb-type pilot arrangement in frequency selective fading channels. *IEEE Transactions on Consumer Electronics*, **44**, 217–225.

[3] Coleri, S., Ergen, M., Puri, A., and Bahai, A. (2002). A study of channel estimation in OFDM systems. In *56th IEEE Vehicular Technology Conference*, pp. 894 – 898.

[4] Schulze, Henrik and Luders, Christian (2005). Theory and applications of OFDM and CDMA, Wiley.

[5] Bingham, J. (1990). Multicarrier modulation for data transmission: an idea whose time has come. *IEEE Communications Magazine*, **28**, 5–14.

[6] Hara, Shinsuke and Prasad, Ramjee (1997). Overview of Multicarrier CDMA. *IEEE Communications Magazine*, **35**, 126–123.

[7] Le-Nous, Sébastien, Nouvel, Fabienne, and Hélard, Jean-François (2004). Design and Implementation of MC-CDMA Systems for Future Wireless Networks. *EURASIP Journal on Applied Signal Processing*, pp. 1604–1615.

[8] Lui, Hui (2000). Signal processing application in CDMA communication, Artech House Publisher.

[9] Hoecher, P., Kaiser, S., and Roberson, P. (1997). Two-dimensional Pilot-Symbol-Aided Channel Estimation by Wienner Filtering. In *IEEE International Conference on Acoustics, Speech, and Signal Processing*, Munich.

[10] Rappaport, Theodore S. (2002). Wireless Communications Principles and Practice, Prentice Hall.

[11] Young, D. J. and Beaulieu, N. C. (2000). The Generation of Correlated Rayleigh Random Variates by Inverse Discrete Fourier Transform. *IEEE Transactions on Communications*, **48**, 1114–1127.

[12] Liu, Hui and Li, Guoqing (2005). OFDM-Based Broadband Wireless Networks, Wiley.

[13] Aldinger, Michael (2005). A Multicarrier Scheme for HIPERLAN, Kluwer Academic Publishers.

[14] IEEE (1999). Part 11: Wireless LAN Medium Access Control (MAC) and Physical Layer (PHY) specifications High-speed Physical Layer in the 5 GHz Band.

[15] 3GPP (2002). TS 25.213v5.0.0, 3rd Generation Partnership Project, Technical Specification Group Radio Access Network, Spreading and modulation (FDD) (Release 5).

List of acronyms

16QAM	16-Level Quadrature Amplitude Modulation
3G	Third Generation
3GPP	Third Generation Partnership Project
4G	Fourth Generation
64QAM	64-Level Quadrature Amplitude Modulation
ADC	Analog to Digital Converter
AWGN	Additive White Gaussian Noise
BER	Bit Error Rate
CDMA	Code Division Multiple Access
DAC	Digital to Analog Converter
DPCCH	Dedicated Physical Control Channel
DPDCH	Dedicated Physical Data Channel
FFT	Fast Fourier Transform
FIR	Finite Impulse Response
FPGA	Field Programmable Gate Array
IFFT	Inverse Fast Fourier Transform
ISI	Inter-Symbol Interference
ICI	Inter-Carrier Interference
ITU	International Telecommunication Union
LDPC	Low Density Parity Check Code
LOS	Line Of Sight
LAN	Local Area Network
LFSR	Linear Feedback Shift Register
MAI	Multiple Access Interference
MC-CDMA	Multi-Carrier Code Division Multiple Access
MFB	Matched Filter Bound
MIMO	Multiple-Input Multiple-Output
OFDM	Orthogonal Frequency Division Multiplexing
OVSF	Orthogonal Variable Spreading Factor
PN	Pseudo Noise
P/S	Parallel-to-Serial
QPSK	Quadrature Phase Shift Keying
SF	Spreading Factor
S/P	Serial-to-Parallel
SNR	Signal-to-Noise Ratio
TS	Technical Specification
UTRA	Universal Terrestrial Radio Access
UARFCN	UTRA Absolute Radio Frequency Channel Number
WCDMA	Wideband Code Division Multiple Access

This page intentionally left blank.

DOCUMENT CONTROL DATA

(Security classification of title, body of abstract and indexing annotation must be entered when document is classified)

1. ORIGINATOR (the name and address of the organization preparing the document. Organizations for whom the document was prepared, e.g. Centre sponsoring a contractor's report, or tasking agency, are entered in section 8.)

   Laboratoire de radiocommunications et de traitement du signal
   Université Laval, Québec

2. SECURITY CLASSIFICATION (overall security classification of the document including special warning terms if applicable).

   UNCLASSIFIED

3. TITLE (the complete document title as indicated on the title page. Its classification should be indicated by the appropriate abbreviation (S,C,R or U) in parentheses after the title).

   Simulation of MC-CDMA systems

4. AUTHORS (last name, first name, middle initial)

   Nguyen, M.-Q.; Fortier, P.; Roy, S.

5. DATE OF PUBLICATION (month and year of publication of document)	6a. NO. OF PAGES (total containing information. Include Annexes, Appendices, etc).	6b. NO. OF REFS (total cited in document)
November 2006	80	15

7. DESCRIPTIVE NOTES (the category of the document, e.g. technical report, technical note or memorandum. If appropriate, enter the type of report, e.g. interim, progress, summary, annual or final. Give the inclusive dates when a specific reporting period is covered).

   Contract Report

8. SPONSORING ACTIVITY (the name of the department project office or laboratory sponsoring the research and development. Include address).

   Defence R&D Canada – Ottawa
   3701, Carling avenue, Ottawa, Ontario, K1A-0Z4

9a. PROJECT NO. (the applicable research and development project number under which the document was written. Specify whether project).	9b. GRANT OR CONTRACT NO. (if appropriate, the applicable number under which the document was written).
15bl11	W7714-5-0942

10a. ORIGINATOR'S DOCUMENT NUMBER (the official document number by which the document is identified by the originating activity. This number must be unique.)	10b. OTHER DOCUMENT NOs. (Any other numbers which may be assigned this document either by the originator or by the sponsor.)
DRDC Ottawa CR 2006-292	

11. DOCUMENT AVAILABILITY (any limitations on further dissemination of the document, other than those imposed by security classification)

   (X) Unlimited distribution
   ( ) Defence departments and defence contractors; further distribution only as approved
   ( ) Defence departments and Canadian defence contractors; further distribution only as approved
   ( ) Government departments and agencies; further distribution only as approved
   ( ) Defence departments; further distribution only as approved
   ( ) Other (please specify):

12. DOCUMENT ANNOUNCEMENT (any limitation to the bibliographic announcement of this document. This will normally correspond to the Document Availability (11). However, where further distribution beyond the audience specified in (11) is possible, a wider announcement audience may be selected).

13. ABSTRACT (a brief and factual summary of the document. It may also appear elsewhere in the body of the document itself. It is highly desirable that the abstract of classified documents be unclassified. Each paragraph of the abstract shall begin with an indication of the security classification of the information in the paragraph (unless the document itself is unclassified) represented as (S), (C), (R), or (U). It is not necessary to include here abstracts in both official languages unless the text is bilingual).

Recently, Orthogonal Frequency Division Multiplexing (OFDM) has become a very attractive multicarrier transmission technique for wireless high speed data communications. OFDM offers robustness to multipath fading without having to provide powerful channel equalization. In order to support multiple users with high speed data communications, the Multi-Carrier Code Division Multiple Access (MC-CDMA) technique is used to address these challenges. MC-CDMA is a combination of OFDM and Code Division Multiple Access (CDMA) and has the benefits of both systems. Thus, the parameters of OFDM become the basic parameters of MC-CDMA. Simulations were performed for an MC-CDMA system under different channel environments. The simulation parameters considered were: guard time interval, symbol duration, sampling rate, and number of data subcarriers. The goal of the simulations was to allow for different MC-CDMA configurations to be tested in order to obtain the best system parameters. Simulations of MC-CDMA systems were also performed with different numbers of active users.

14. KEYWORDS, DESCRIPTORS or IDENTIFIERS (technically meaningful terms or short phrases that characterize a document and could be helpful in cataloguing the document. They should be selected so that no security classification is required. Identifiers, such as equipment model designation, trade name, military project code name, geographic location may also be included. If possible keywords should be selected from a published thesaurus. e.g. Thesaurus of Engineering and Scientific Terms (TEST) and that thesaurus-identified. If it not possible to select indexing terms which are Unclassified, the classification of each should be indicated as with the title).

OFDM
pilot tone
channel estimation
MC-CDMA
spreading
channelisation
scrambling

Defence R&D Canada

Canada's leader in Defence
and National Security
Science and Technology

R & D pour la défense Canada

Chef de file au Canada en matière
de science et de technologie pour
la défense et la sécurité nationale

www.drdc-rddc.gc.ca